Article

Molecular Cell

An Attachment-Independent Biochemical Timer of the Spindle Assembly Checkpoint

Graphical Abstract

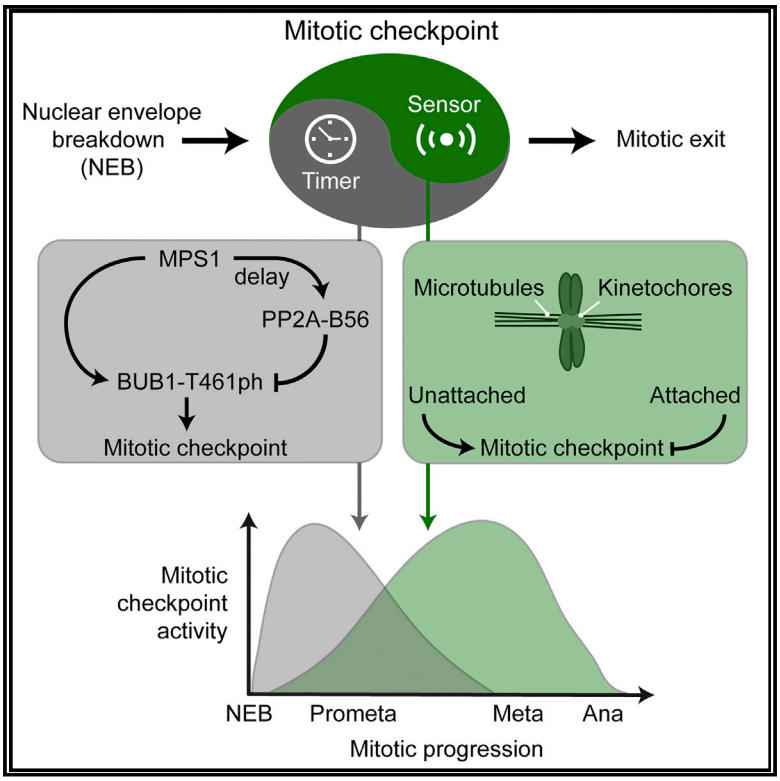

Highlights

- Pulse phosphorylation of BUB1 transiently promotes MAD1 kinetochore recruitment
- Phosphorylation of BUB1 by MPS1 is reversed by BUBR1-associated PP2A-B56
- Delayed PP2A-B56 recruitment shapes an attachment-independent timer
- Targeting cancer cells by disrupting the BUB1 timer holds therapeutic potential

Authors

Junbin Qian, Maria Adelaida García-Gimeno, Monique Beullens, ..., Pascual Sanz, Lendert Gelens, Mathieu Bollen

Correspondence

junbin.qian@kuleuven.be (J.Q.), mathieu.bollen@kuleuven.be (M.B.)

In Brief

Qian et al. show that the spindle assembly checkpoint is governed by consecutive timer and sensor mechanisms. The timer involves the attachment-independent pulse phosphorylation of BUB1. They propose that the timer serves to activate the checkpoint before attachment-dependent sensor mechanisms become operational.

Qian et al., 2017, Molecular Cell *68*, 1–16
November 16, 2017
https://doi.org/10.1016/j.molcel.2017.10.011

CellPress

Please cite this article in press as: Qian et al., An Attachment-Independent Biochemical Timer of the Spindle Assembly Checkpoint, Molecular Cell (2017), https://doi.org/10.1016/j.molcel.2017.10.011

Molecular Cell
Article

CellPress

An Attachment-Independent Biochemical Timer of the Spindle Assembly Checkpoint

Junbin Qian,[1,*] Maria Adelaida García-Gimeno,[2] Monique Beullens,[1] Maria Giulia Manzione,[1] Gerd Van der Hoeven,[1] Juan Carlos Igual,[3] Miguel Heredia,[4] Pascual Sanz,[4] Lendert Gelens,[5] and Mathieu Bollen[1,6,*]
[1]Laboratory of Biosignaling & Therapeutics, Department of Cellular and Molecular Medicine, University of Leuven, 3000 Leuven, Belgium
[2]Departament de Biotecnologia, Universitat Politècnica de València, Camino de Vera, 14, 46022 Valencia, Spain
[3]Departament de Bioquímica i Biologia Molecular and Estructura de Recerca Interdisciplinar en Biotecnologia i Biomedicina (ERI BIOTECMED), Universitat de València, 46100 Burjassot (Valencia), Spain
[4]Instituto de Biomedicina de Valencia (CSIC), Centro de Investigación Biomédica en Red de Enfermedades Raras (CIBERER), Jaime Roig 11, 46010 Valencia, Spain
[5]Laboratory of Dynamics in Biological Systems, Department of Cellular and Molecular Medicine, University of Leuven, 3000 Leuven, Belgium
[6]Lead Contact
*Correspondence: junbin.qian@kuleuven.be (J.Q.), mathieu.bollen@kuleuven.be (M.B.)
https://doi.org/10.1016/j.molcel.2017.10.011

SUMMARY

The spindle assembly checkpoint (SAC) generates a diffusible protein complex that prevents anaphase until all chromosomes are properly attached to spindle microtubules. A key step in SAC initiation is the recruitment of MAD1 to kinetochores, which is generally thought to be governed by the microtubule-kinetochore (MT-KT) attachment status. However, we demonstrate that the recruitment of MAD1 via BUB1, a conserved kinetochore receptor, is not affected by MT-KT interactions in human cells. Instead, BUB1:MAD1 interaction depends on BUB1 phosphorylation, which is controlled by a biochemical timer that integrates counteracting kinase and phosphatase effects on BUB1 into a pulse-generating incoherent feedforward loop. We propose that this attachment-independent timer serves to rapidly activate the SAC at mitotic entry, before the attachment-sensing MAD1 receptors have become fully operational. The BUB1-centered timer is largely impervious to conventional anti-mitotic drugs, and it is, therefore, a promising therapeutic target to induce cell death through permanent SAC activation.

INTRODUCTION

The spindle assembly checkpoint (SAC) is a eukaryotic safeguard mechanism that ensures accurate chromosome segregation during cell division (for references see Musacchio, 2015). It monitors interactions between spindle microtubules and the chromosome-associated kinetochore complex, and it prevents the onset of anaphase as long as unattached or incorrectly attached kinetochores are detected. The SAC effector is the mitotic checkpoint complex (MCC), which consists of MAD2, BUBR1, BUB3, and CDC20. By sequestering CDC20, the MCC prevents activation of the anaphase-promoting complex/cyclosome (APC/C), which initiates anaphase by targeting cyclin B1 and securin for proteasomal degradation. After nuclear envelope breakdown (NEB), kinetochores serve as platforms for the stepwise assembly of the MCC. Initially, MAD1 and a conformer of MAD2, known as closed-MAD2 (C-MAD2), are recruited to unattached kinetochores. The MAD1:C-MAD2 complex acts as a scaffold to recruit cytosolic open-MAD2 (O-MAD2) and convert it to C-MAD2. C-MAD2 binds to CDC20 and the resulting complex is the immediate precursor for MCC assembly.

In budding yeast, the only kinetochore receptor for Mad1 is Bub1 (Heinrich et al., 2014; London and Biggins, 2014). Protein kinase Mps1 promotes Bub1:Mad1 interaction through Bub1 phosphorylation. An interaction between the human MAD1 and BUB1 orthologs has also been demonstrated *in vitro*, but it has not been confirmed by co-immunoprecipitation (Faesen et al., 2017; Ji et al., 2017; Zhang et al., 2017). Actually, the contribution of BUB1 to MAD1 recruitment in mammalian cells is highly controversial (Hewitt et al., 2010; Kim et al., 2012; Klebig et al., 2009; Liu et al., 2006; Silió et al., 2015; Vleugel et al., 2013, 2015a; Zhang et al., 2015), and it is further confounded by the existence of two additional MAD1 receptors, namely, CEP57 and the ROD, ZW10, and ZWILCH (RZZ) complex (Kops et al., 2005; Zhou et al., 2016). It is currently unclear whether the mammalian MAD1 receptors act redundantly or in distinct circumstances.

Here we show that BUB1:MAD1 interaction in human cells only occurs in early mitosis and is lost during prolonged prometaphase. We also demonstrate that BUB1:MAD1 interaction is transient because of a delayed recruitment of the phosphatase (PP2A-B56) that dephosphorylates BUB1 at a site that is critical for MAD1 interaction. Intriguingly, PP2A-B56-mediated dephosphorylation of BUB1 is not affected by the microtubule-kinetochore (MT-KT) attachment status, but it is controlled by a biochemical timer. This attachment-independent timer, which is largely insensitive to conventional SAC-activating drugs, is essential for SAC signaling and, therefore, an attractive target for the induction of mitotic cell death in cancer cells.

Please cite this article in press as: Qian et al., An Attachment-Independent Biochemical Timer of the Spindle Assembly Checkpoint, Molecular Cell (2017), https://doi.org/10.1016/j.molcel.2017.10.011

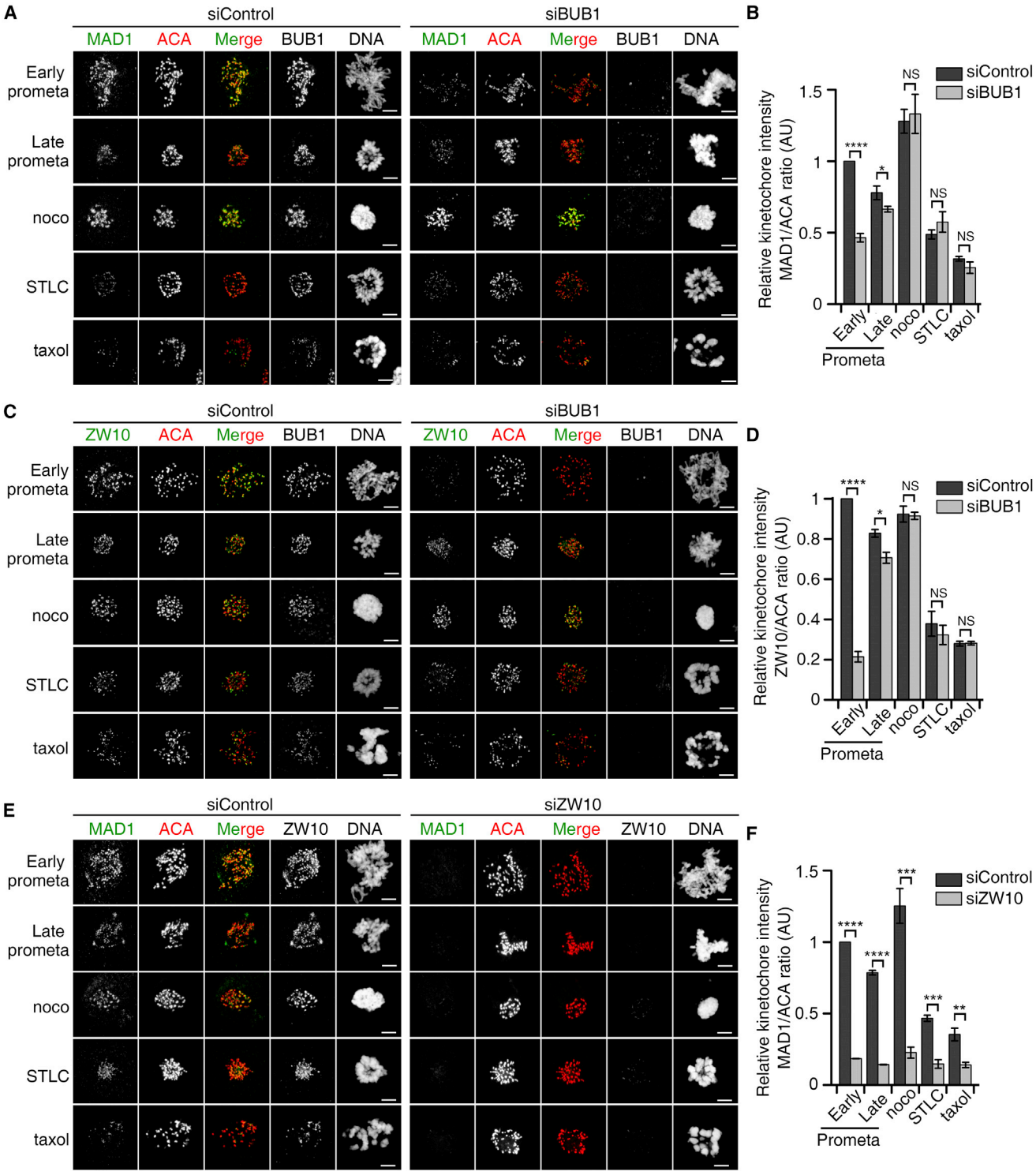

Figure 1. BUB1 Is Required for MAD1/RZZ Recruitment in Early Mitosis

(A) HeLa cells treated with control (siControl) or BUB1 (siBUB1) siRNA were synchronized to late G2 by sequential thymidine-RO3306 treatment and released into fresh medium for 10–20 min (early mitosis) or into medium containing MG132 and nocodazole (noco), STLC, or taxol. After 3 hr, cells were fixed and (immuno) stained.

(B) Quantification of the kinetochore MAD1/ACA ratio in (A).

(C) Same as (A) except for different antibody stainings.

(legend continued on next page)

RESULTS

BUB1 Is Only Transiently Required for MAD1 and ZW10 Kinetochore Recruitment

BUB1 kinetochore targeting in HeLa cells already started in late G2, when chromatin was still uncondensed and only histone H3 near the nuclear rim was phosphorylated at Ser10 (Figures S1A and S1B). ZW10 was recruited in late prophase, when MAD1 was still associated with the nuclear envelope (Figure S1C), and MAD1 only became associated with the kinetochores after nuclear envelope breakdown (Figure S1C). These findings hinted at a hierarchal recruitment mechanism, and they prompted us to examine the interdependence of BUB1, ZW10, and MAD1 kinetochore recruitment, using previously validated small interfering RNAs (siRNAs) (Figure S1D; Table S1). Others have used a similar approach but with conflicting outcomes (Hewitt et al., 2010; Kim et al., 2012; Klebig et al., 2009; Liu et al., 2006; Silió et al., 2015; Vleugel et al., 2013, 2015a; Zhang et al., 2015). To determine whether these discrepant findings can be explained by different synchronization protocols and/or a focus on different phases of mitosis, we compared 5 distinct conditions: (1) early prometaphase (stretched chromosomes after NEB), (2) late prometaphase (condensed chromosomes without a metaphase plate), (3) nocodazole arrest (lack of MT-KT interactions), (4) S-trityl-L-cysteine (STLC) arrest (monopolar spindle and lateral MT-KT interactions), and (5) taxol arrest (transient end-on MT-KT attachments). Strikingly, BUB1 knockdown reduced MAD1 and ZW10 kinetochore recruitment in prometaphase, especially in early prometaphase, but not in cells that had been blocked with spindle poisons (Figures 1A–1D). This suggests that, regardless of the MT-KT interaction status, BUB1 is required for the initial recruitment of ZW10 and MAD1, but not after prolonged prometaphase arrest. ZW10 knockdown significantly compromised MAD1 kinetochore localization in all tested conditions (Figures 1E and 1F), but it did not affect BUB1 localization (Figures S1E and S1F). Finally, MAD1 depletion did not impact ZW10 kinetochore localization in any condition, apart from a small reduction in early prometaphase (Figures S1G and S1H). Thus, kinetochore localization of MAD1 is dependent on both BUB1 and ZW10, and BUB1 only transiently contributes to MAD1 and ZW10 recruitment.

BUB1-Mediated MAD1 and CDC20 Recruitment Is Essential for CDC20:MAD2 Assembly

Since BUB1 was only transiently required for MAD1 recruitment, we examined whether a BUB1:MAD1 complex can be detected in early mitosis. HeLa cells were synchronized in late G2 by sequential treatment with thymidine and the CDK1 inhibitor RO3306, and they were allowed to enter mitosis by RO3306 washout. MAD1 co-immunoprecipitated with BUB1 after RO3306 release, and maximal interaction was observed 15 min after release (Figure 2A). Reduced BUB1:MAD1 interaction at 30 min preceded cyclin B1 degradation, confirming that the BUB1:MAD1 interaction is transient and lost before metaphase completion. To explore the importance of this transient BUB1:MAD1 interaction for SAC signaling, we measured SAC strength by quantifying the amount of MAD2 that co-immunoprecipitates with CDC20. After RO3306 washout, CDC20:MAD2 interaction steadily increased for 30 min and subsequently decreased (Figure 2B). However, in BUB1-depleted cells, the increase in CDC20:MAD2 interaction was slower and less pronounced, suggesting that BUB1 makes a quantitatively important contribution to CDC20:MAD2 interaction in early mitosis. BUB1 knockdown also reduced BUBR1 binding to CDC20 but to a lesser extent.

Deletion of the conserved CD1 domain of BUB1 (residues 458–476 of human BUB1) reduces MAD1 kinetochore localization (Klebig et al., 2009; Zhang et al., 2015). We confirmed this observation using isogenic HeLa Flp-in T-REx cell lines after knockdown of endogenous BUB1 and expression of mClover-tagged wild-type (WT) BUB1 or a mutant BUB1 with the CD1 domain deleted (ΔCD1) (Figures S2A and S2B). The 17 amino acids N-terminal to the CD1 domain are also conserved in vertebrates (see below), and the combined deletion of these 17 residues and the CD1 domain (residues 441–476) further reduced the recruitment of MAD1 in early prometaphase. Hence, the latter mutant can be used as a MAD1-binding mutant (BUB1-ΔMAD1).

BUB1-mediated kinetochore recruitment of MAD1:C-MAD2 facilitates the recruitment of O-MAD2 and its catalytic conversion to C-MAD2 (Caldas et al., 2015; Faesen et al., 2017; Ji et al., 2017; Zhang et al., 2015). However, BUB1 has also been proposed to contribute to APC/C inhibition, in parallel but not redundant to MCC formation, through CDC20 phosphorylation (Jia et al., 2016). To delineate the relative importance of MAD1 and CDC20 recruitment by BUB1, in the absence of CDC20 phosphorylation, we generated HeLa Flp-in T-REx stable cell lines that express variants of an N-terminal BUB1 fragment (residues 1–556; lacking the kinase domain and PLK1-binding site) fused to mClover. The BUB1 fragment was WT, lacking the MAD1-binding site (residues 441–476; ΔMAD1), and/or lacking the CDC20-binding site (residues 527–537; ΔCDC20) (Di Fiore et al., 2015). After endogenous BUB1 knockdown, BUB1-ΔMAD1 and BUB1-ΔCDC20 expression compromised the kinetochore recruitment of MAD1 and CDC20, respectively, in early prometaphase, as compared to BUB1-WT-expressing cells (Figures 2C and 2D). BUB1-ΔMAD1 expression also reduced CDC20 recruitment by a quarter, confirming that the MAD1:BUB1:CDC20 complex assembly is cooperative (Faesen et al., 2017; Ji et al., 2017). However, this effect of BUB1-ΔMAD1 expression on CDC20 recruitment was lost during prolonged mitosis in nocodazole-arrested cells (Figures S2C and S2D), hinting at a transient nature of MAD1:CDC20 interaction.

To compare the effect of the truncated BUB1 variants on SAC strength, we first measured cyclin B1 levels in cells that were

(D) Quantification of the kinetochore ZW10/ACA ratio in (C).

(E) Cells were treated as in (A), but a ZW10-specific siRNA (siZW10) was used instead of siBUB1.

(F) Quantification of the kinetochore MAD1/ACA ratio in (E).

Scale bar, 5 μm (A, C, and E). In (B), (D), and (F), the data represent mean ± SEM (n = 3, ≥10 cells/condition/experiment). See also Figure S1.

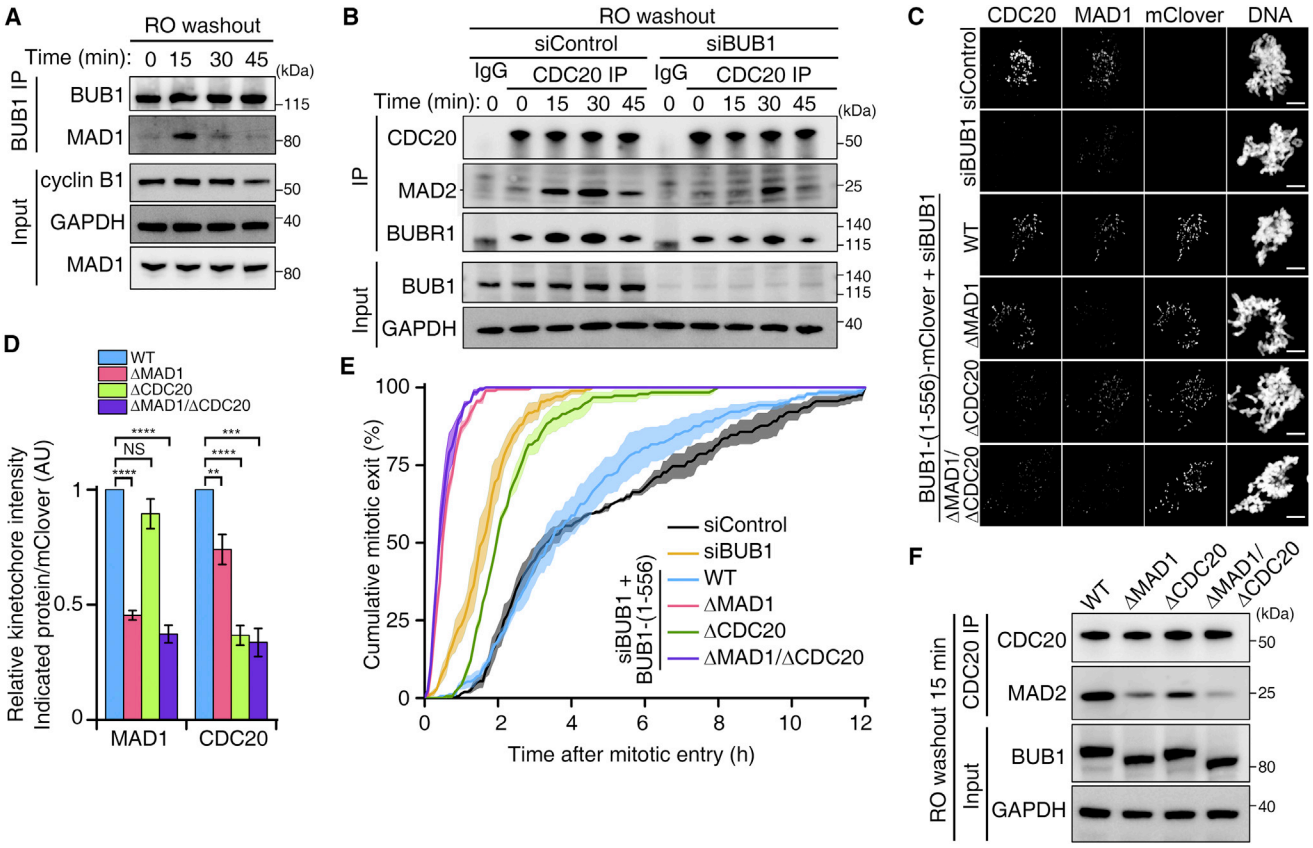

Figure 2. BUB1 Is Required for SAC and CDC20:MAD2 Assembly

(A) HeLa cells were synchronized by sequential thymidine-RO3306 treatment and released into fresh medium prior to BUB1 immunoprecipitation.

(B) Cells were synchronized as in (A) and treated with control (siControl) or BUB1 (siBUB1) siRNA prior to CDC20 immunoprecipitation.

(C) HeLa cells expressing BUB1-(1-556)-mClover WT or the indicated deletion mutants were synchronized to early prometaphase and (immuno)stained. Scale bar, 5 μm.

(D) Quantification of the MAD1/mClover and CDC20/mClover ratio in (C). The data represent mean ± SEM (n = 3, ≥10 cells/condition/experiment).

(E) Time-lapse analysis of the duration of mitosis in HeLa cells expressing mClover-tagged BUB1-(1-556) WT or the indicated mutants. Cells were transfected with control (siControl) or BUB1 (siBUB1) siRNA, synchronized with thymidine for 24 hr, and released into fresh medium for 6 hr before taxol treatment and time-lapse differential interference contrast (DIC) imaging. The data show cumulative percentages of mitotic exit cells ± SEM (n = 3, ≥53 cells/condition/experiment).

(F) HeLa Flp-in T-REx cells expressing BUB1-(1-556)-mClover WT or the indicated mutants were synchronized as in (B) and treated with a BUB1 siRNA. CDC20 was immunoprecipitated 15 min after release from RO3306 arrest.

See also Figure S2.

SAC arrested with taxol. Cyclin B1 levels were reduced after endogenous BUB1 knockdown and taxol treatment, consistent with an early mitotic exit due to a SAC defect (Figure S2E, left panel). This effect was largely rescued by expression of the BUB1-WT fragment. However, the phenotype was not rescued by BUB1-ΔCDC20, and it was even aggravated by BUB1-ΔMAD1 or BUB1-ΔMAD1/ΔCDC20. This indicates that BUB1-associated CDC20 and MAD1 are required for the SAC. Our data also suggest that BUB1-ΔMAD1 and BUB1-ΔMAD1/ΔCDC20 act in a dominant-negative manner, as has also been proposed for another N-terminal BUB1 fragment (Klebig et al., 2009; Taylor and McKeon, 1997). The expression of the BUB1 deletion mutants was reduced in taxol-arrested cells. This is consistent with an increased proportion of cells in interphase when BUB1 expression is much lower (Qi and Yu, 2007). In support of this, all BUB1 variants were expressed at similar levels in cells that were mitotically enriched by nocodazole treatment and mitotic shake-off (Figure S2E, right panel).

To validate the SAC data in single cells, we measured the duration of mitosis in taxol-treated cells using time-lapse imaging (Figure 2E). BUB1 knockdown reduced the mitotic duration of taxol-arrested cells, and this phenotype was rescued by the expression of BUB1-(1-556)-WT, but not by the corresponding BUB1-ΔCDC20 mutant. Consistent with the dominant-negative effect of BUB1-ΔMAD1 and BUB1-ΔMAD1/ΔCDC20 on cyclin B1 (Figure S2E, left panel), their expression also impaired the SAC more than the knockdown of endogenous BUB1 (Figure 2E). This dominant-negative effect could be taken as evidence that the BUB1 knockdown was incomplete and that residual BUB1 contributes to the BUB1-independent phenotype for MAD1 recruitment in mitotically arrested cells (Figure 1A). However, we did not observe any difference in

MAD1 localization in nocodazole-arrested cells with knockdown of endogenous BUB1 and expression of either BUB1-WT or BUB1-ΔMAD1 (Figures S2F and S2G), indicating that residual BUB1 does not account for MAD1 recruitment in mitotically arrested cells. Finally, we found that the SAC defect induced by BUB1-ΔMAD1 and BUB1-ΔCDC20 correlated with a reduced co-immunoprecipitation of MAD2 with CDC20 (Figure 2F). We conclude that BUB1 promotes SAC activation by enhancing CDC20:MAD2 assembly and this requires BUB1 binding to both MAD1 and CDC20.

Phosphorylation of the Extended CD1 Domain of BUB1 Is Required for SAC Initiation

The CD1 domain of BUB1 (residues 458–476) is conserved from yeast to man, but the N-terminal flanking region (residues 441–457) is only conserved in vertebrates (Figure S3A). Within the CD1 domain, human BUB1 is phosphorylated at S459 by CDK1, which primes T461 phosphorylation by MPS1 (Ji et al., 2017; Zhang et al., 2017). Immunostaining with a phospho-epitope-specific antibody raised against a T461-phosphorylated BUB1 peptide confirmed BUB1-T461 phosphorylation in early prometaphase (Figure S3B), which was prevented by the inhibition of MPS1 with reversine (Figures 3A and 3B). Reversine also reduced BUB1 kinetochore recruitment, which could result from decreased phosphorylation of the KNL1 MELT motifs by MPS1 and an associated loss of phospho-MELT docking sites for BUB1:BUB3. However, the T461ph signal was also completely lost in a subset of reversine-treated cells that still showed significant levels of kinetochore-associated BUB1. This suggests that the role of MPS1 in T461 phosphorylation is, at least in part, independent of its contribution to BUB1 kinetochore recruitment.

We also confirmed that the phosphorylation of BUB1 by MPS1 was dependent on CDK-mediated priming phosphorylation at T459, both *in vitro* (Figures S3C and S3D) and in intact cells (Figure S3E). BUB1 also contains other consensus CDK phosphorylation sites, including T441 and T452 in the extended CD1 domain (Figure S3A). We found that *in vitro* phosphorylation of human BUB1-(437-509) by CDK2 was abolished when all three CDK consensus sites (T441, T452, and S459) were mutated to alanine (BUB1-3A; Figure S3F). T441 and T452 are followed by a proline and their phosphorylation can be visualized with a pan-phospho-TP antibody. mClover-tagged BUB1-(1-556)-WT stained positive with the pan-phospho-TP antibody in mitotic cells, but not in non-synchronized cells (Figure S3G). Furthermore, mitotic phosphorylation was not detected with the BUB1-3A mutant. These data indicate that T441 and/or T452 is also phosphorylated by CDK1 during mitosis. Finally, the prior CDK phosphorylation of budding yeast Bub1-(353-555) also promoted its subsequent phosphorylation by MPS1 (Figure S3H), showing that CDK-primed phosphorylation of BUB1/Bub1 by MPS1 is conserved from yeast to mammals.

We subsequently explored whether T461 phosphorylation of human BUB1 contributes to BUB1:MAD1 interaction. Purified BUB1-(437-509) was phosphorylated with CDK2 or CDK2+MPS1 before *in vitro* pull-downs with a recombinant His-tagged C-terminal domain (CTD) fragment of MAD1 (Figure 3C). Phosphorylation of this BUB1 fragment by CDK2 only slightly promoted its interaction with MAD1, while the sequential phosphorylation by CDK2 and MPS1 dramatically increased the BUB1:MAD1 interaction. In the latter condition, the ability of BUB1 to bind MAD1 correlated positively with the phosphorylation level of T461. Moreover, the T461A mutation largely abolished the binding of BUB1-(437-509) to MAD1 (Figure 3D). We also found that BUB1 was more phosphorylated at T461 in the chromosomal fraction from early mitotic cells, as compared to the cytosolic fraction, and this correlated with a higher co-immunoprecipitation of MAD1 in the chromosomal fraction (Figure S3I). Using HeLa Flp-in T-REx cell lines that stably express siRNA-resistant and Venus-tagged BUB1 (mutants), the association of MAD1 with the kinetochores during early prometaphase was one-third lower in cells expressing the non-phosphorylatable mutant BUB1-T461A, as compared to cells that expressed BUB1-WT (Figures 3E and 3F). However, MAD1 kinetochore recruitment was not affected by the phosphomimetic BUB1-T461E. Collectively, our data demonstrate that T461 phosphorylation is required for efficient MAD1 recruitment, both *in vitro* and in cells. In budding yeast, we also detected an interaction between Bub1 and Mad1 using two-hybrid assays (Figure 3G). This interaction was lost in Bub1-S451A and Bub1-T453A mutant strains, but it was retained in strains expressing the Bub1-S451E or Bub1-T453E mutants. These data are consistent with a requirement of Bub1-S451 and Bub1-T453 phosphorylation for Mad1 interaction.

To quantify the contribution of BUB1 phosphorylation to SAC activation, we generated HeLa Flp-in T-REx stable cell lines that express human Venus-tagged BUB1-WT or non-phosphorylatable mutants, and we examined the SAC phenotype after endogenous BUB1 knockdown (Figure S3J). A defective SAC, indicated by reduced cyclin B1 levels, was observed in taxol-treated cells that expressed BUB1-S459A, BUB1-T461A, BUB1-S459A/T461A (BUB1-2A), or BUB1-T441A/T452A/S459A (BUB1-3A). Single-cell time-lapse imaging analysis confirmed that the expression of these BUB1 mutants was associated with an impaired SAC (Figure 3H). The S459A mutation had a stronger SAC-compromising effect than the T461A mutation, consistent with the notion that S459 phosphorylation contributes to the BUB1:MAD1 interaction both directly and indirectly, through priming of T461 phosphorylation by MPS1 (Ji et al., 2017). The BUB1-3A mutant had an even more extreme phenotype than the S459A mutant, indicating that phosphorylation at T441 and T452 also contributes to SAC activation.

Budding yeast with a defective SAC is sensitive to microtubule-destabilizing drugs (London and Biggins, 2014). In the presence of nocodazole, Bub1 WT or the phosphomimetic Bub1-S451E or Bub1-T453E rescued cell growth of *bub1Δ* cells, and the rescued cells accumulated with a big bud and a single nucleus in G2/M (Figure S3K). However, cell growth was not rescued by Bub1-S451A or Bub1-T453A expression (Figure 3I), suggesting that these mutations are associated with a compromised SAC. Expression of a PP1-binding mutant (RASA) of Spc105 (ortholog to human KNL1) causes a growth defect due to constitutive activation of the SAC (Rosenberg et al., 2011), which could be rescued by Bub1 deletion (Figure 3J). We found

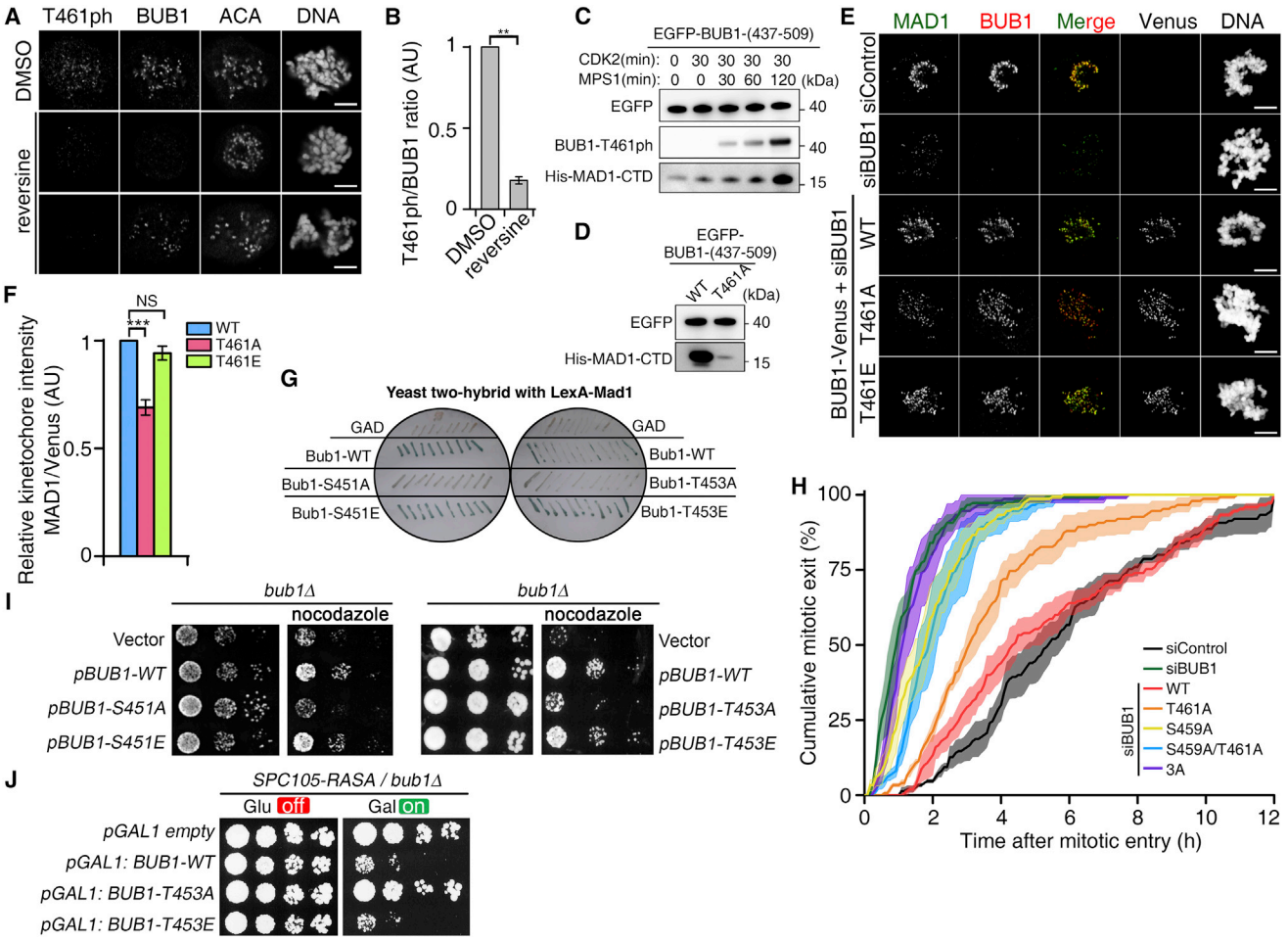

Figure 3. BUB1 Phosphorylation by CDK1 and MPS1 Promotes SAC Activation

(A) HeLa cells were released from a RO3306 arrest and treated with 250 nM reversine or vehicle (DMSO) for 20 min. Early prometaphase T461ph was visualized by immunostaining.

(B) Quantification of the T461ph/BUB1 ratio from cells that retained kinetochore-associated BUB1 in (A). The data represent mean ± SEM (n = 3, ≥10 cells/condition/experiment).

(C) Traps of human EGFP-BUB1-(437-509) were incubated for 0 or 30 min with CDK2 before phosphorylation with MPS1 for the indicated time points. Subsequently, the traps were used for immunoblotting and pull-down with recombinant His-tagged MAD1-CTD.

(D) Traps of EGFP-BUB1-(437-509) WT or T461A were phosphorylated by CDK2 plus MPS1 before pull-down with recombinant His-tagged MAD1-CTD.

(E) HeLa cells expressing Venus-tagged BUB1 WT or the indicated mutants were treated with control (siControl) or BUB1 siRNA (siBUB1) and released from RO3306 for 20 min before (immuno)staining.

(F) Quantification of the MAD1/Venus ratio in (E). The data are mean ± SEM (n = 3, ≥10 cells/condition/experiment).

(G) Yeast two-hybrid analysis of yeast Mad1 and Bub1 mutant interaction. Yeast cells co-expressed a LexA-Mad1 and GAD-Bub1 variants.

(H) Time-lapse analysis of the duration of mitosis in taxol-treated cells expressing mClover-tagged BUB1-(1-556) WT or the indicated mutants. The data show cumulative percentages of mitotic exit cells ± SEM (n = 3, ≥50 cells/condition/experiment).

(I) Three-fold serial dilutions of *bub1Δ* yeast cells transformed with a plasmid expressing Bub1-WT or the indicated point mutants, under the control of the endogenous *BUB1* promoter, were spotted on YP-Galactose medium with or without nocodazole (13.2 μM) and incubated for 2–3 days at 25°C.

(J) Four-fold serial dilutions of the yeast *SPC105 RASA/bub1Δ* strains expressing Bub1-WT, Bub1-T453A, or Bub1-T453E, under the control of *GAL1* promoter, were spotted on YP-Glucose (Glu) medium or YP-Galactose (Gal) medium and incubated at 25°C for 3 or 4 days.

Scale bar, 5 μm (A and E). See also Figure S3.

that the growth of a *SPC105-RASA/bub1Δ* strain was inhibited by Bub1-WT or Bub1-T453E expression, but not by Bub1-T453A expression. These data indicate that Bub1-T453 phosphorylation plays an essential role in SAC activation. Thus, SAC activation by BUB1/Bub1 CD1 domain phosphorylation is conserved from yeast to man.

BUB1-T461 Is Dephosphorylated by BUBR1-Associated PP2A-B56

BUB1-T461 phosphorylation was already detected in early prophase, reached a maximum in late prophase, started to decrease after NEB, and became undetectable in metaphase (Figures 4A and 4B). Remarkably, T461 phosphorylation was

barely detectable after a prolonged prometaphase arrest, which correlated with a loss of BUB1:MAD1 interaction in these conditions (Figures 1A and 1B). A similar pulse of T461 phosphorylation was detected in non-transformed RPE-1 cells (Figure S4A). These data suggest that T461 phosphorylation is tightly coupled to the timely progression of mitosis but is independent of the MT-KT attachment status. We also looked at the dynamics of S459 phosphorylation, using a published antibody (Ji et al., 2017) that was re-examined for specificity (Figure S4B). S459 was barely dephosphorylated in late prometaphase or in the presence of spindle poisons (Figures S4C and S4D), in contrast to what we observed for T461. This suggests that T461 phosphorylation, which is more dynamic, is the determining factor for BUB1:MAD1 interaction.

The transient nature of BUB1-T461 phosphorylation prompted us to identify the phosphatase(s) involved in dephosphorylation. Treatment of nocodazole-arrested HeLa cells with calyculin A, an inhibitor of PP1 and PP2A (like) phosphatases, increased BUB1 phosphorylation at T461 (Figure 4C). Similarly, BUB1-T461 phosphorylation was increased by knockdown of the catalytic (α isoform) or B56 subunits (all isoforms) of PP2A, but it was not affected by knockdown of the catalytic subunit of PP1 (all isoforms) or the B55 subunit of PP2A (α and δ isoforms; Figures 4D–4F). This suggests that BUB1-T461 is dephosphorylated by a pool of PP2A-B56.

PP2A-B56 is recruited to the kinetochores via the KARD domain of BUBR1 (Kruse et al., 2013; Suijkerbuijk et al., 2012). BUBR1 with a deleted KARD domain (ΔKARD) functions as a PP2A-B56-binding mutant. Using stable HeLa cell lines that inducibly express BUBR1-WT or BUBR1-ΔKARD (Figure S4E), we found that the phosphorylation of BUB1-T461 was dramatically increased when endogenous BUBR1 was replaced by BUBR1-ΔKARD. This increase was detected in both nocodazole-arrested (Figures 4G and 4H) and late prometaphase cells (Figure S4F), and it was associated with an increased BUB1:MAD1 interaction (Figure S4G). Also, MPS1-phosphorylated BUB1-(437-509) was dephosphorylated *in vitro* by BUBR1-WT traps that contained PP2A-B56, which was not seen with BUBR1-ΔKARD traps (Figure 4I). Together, these data strongly suggest that BUBR1 recruits PP2A-B56 to dephosphorylate BUB1 at T461.

Profile of the BUB1-T461 Phosphorylation Pulse

MPS1 phosphorylates BUB1 at T461, thereby promoting MAD1 recruitment (Figure 5A). However, MPS1 also phosphorylates the MELT repeats of KNL1, resulting in the recruitment of BUB proteins and associated PP2A-B56, which dephosphorylates BUB1 at T461. Hence, MPS1 signaling induces an incoherent type-1 feedforward loop that can generate a biphasic response (Mangan and Alon, 2003). The shape of this BUB1-targeted pulse response is largely determined by three parameters (Figure 5B): the BUB1 phosphorylation rate (r_p), the BUB1 dephosphorylation rate (r_d), and the time delay (T_{delay}) in phosphatase recruitment (or activation).

Using these basic components, we simulated BUB1-T461 phosphorylation kinetics in different conditions (Figure 5C). In the absence of counteracting PP2A-B56, T461 was quickly phosphorylated by MPS1 (green curve). When the phosphatase and kinase were activated simultaneously (no time delay, T = 0), T461 phosphorylation was slowed and limited to a maximal phosphorylation of 50% when r_p was equal to r_d (Figure 5C, left panel, black curve). However, if the phosphatase was more active, e.g., r_d was 10 times r_p, T461 only showed a net phosphorylation of 10% (Figure 5C, right panel, black curve). Finally, if the phosphatase was only activated after a time delay, T, a biphasic response emerged (red curve). Initially, the kinase was able to quickly phosphorylate T461 (green curve); but, when the counteracting phosphatase was activated after a time delay, the system relaxed back to the phosphorylation level indicated by the black curve. The transient pulse had an amplitude that increased with longer time delays before phosphatase recruitment/activation and decayed more quickly with higher phosphatase/kinase activity ratios (Figure 5C, right panel, red curve). Our data on mitotic BUB1-T461 phosphorylation are consistent with delayed recruitment/activation of PP2A-B56 at the kinetochores and a high PP2A-B56/MPS1 activity ratio during the pulse-decay phase (Figure 4B).

Although MPS1 is already active in prophase, PP2A-B56 is only recruited to kinetochore-associated BUBR1 in prometaphase because multiple steps are required (Figures 5A and S5A). First, the MELT motifs of KNL1 have to be phosphorylated, which serve as (indirect) docking sites for BUBR1 (Nijenhuis et al., 2014). However, BUBR1 is excluded from the nucleus and so it can only be recruited after NEB. Once BUBR1:KNL1 interaction has been established, the BUBR1 KARD domain is phosphorylated by CDK1 and PLK1, which is required for the recruitment of PP2A-B56 (Kruse et al., 2013; Suijkerbuijk et al., 2012). Phosphorylation of the KARD domain probably only occurs after BUBR1 kinetochore recruitment because a BUBR1 kinetochore-binding mutant protein is not phosphorylated (Elowe et al., 2010). Using a simple simulation, we found that, as the number of intermediate steps increases, the delay in the PP2A-B56 kinetochore recruitment increases and recruitment also becomes more gradual (Figure 5D, upper panel). Delayed PP2A-B56 recruitment ensured a smooth pulse of BUB1-T461 phosphorylation, with a maximum that increased with the length of the time delay (Figure 5D, lower panel).

To experimentally validate our simulations, we released RO3306-arrested HeLa cells for different time points, and we immunoprecipitated BUB1 and BUBR1. Phosphorylation of BUB1 at T461 (T461ph) correlated with BUB1:MAD1 binding, which both peaked at 15 min and diminished afterward (Figure 5E). In contrast, phosphorylation of the BUBR1 KARD domain at S670 (S670ph), which mediates the recruitment of PP2A-B56, took off much more slowly and only peaked at 30 min. The recruitment of PP2A-B56 closely followed the pattern of S670 phosphorylation. BUBR1 phosphorylation at S670 was barely detectable in early prometaphase, increased during late prometaphase, and peaked during prolonged mitosis in nocodazole-arrested cells (Figure S5B). This is different from the kinetics of BUB1 phosphorylation at T461 (Figures 4A, 4B, and S5C), but it is consistent with our conclusion that the dephosphorylation of this site is mediated by BUBR1-associated PP2A-B56 (Figure 4). These validation data fully support the notion that the BUB1-T461 phosphorylation pulse is generated through an incoherent feedforward loop encoded by a

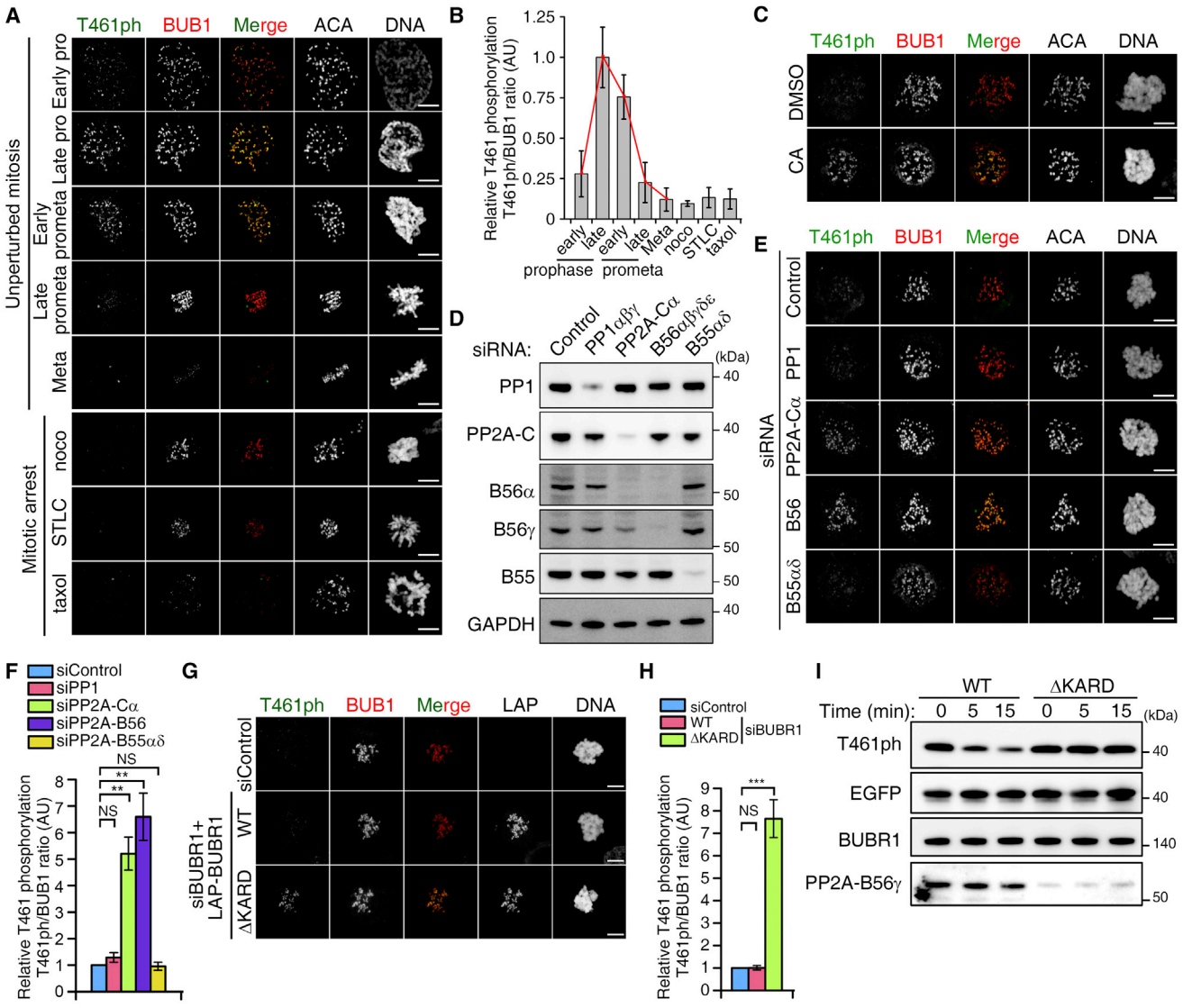

Figure 4. T461 Dephosphorylation Is Dependent on BUBR1:PP2A-B56

(A) HeLa cells in different mitotic phases or arrested in nocodazole, STLC, or taxol were stained.

(B) Quantification of the T461ph/BUB1 ratio in (A). The data represent the mean ± SD for at least 10 cells/condition.

(C) Nocodazole-arrested HeLa cells were treated with 20 nM calyculin A for 20 min prior to fixation and (immuno)staining.

(D) Efficacy of knockdown of PP1 (all isoforms), PP2A-Cα, B56 (all isoforms), and B55 (αδ isoforms) in HeLa cells.

(E) (Immuno)staining of nocodazole-arrested HeLa cells transfected with the same siRNAs as in (D).

(F) Quantification of the T461ph/BUB1 ratio in (E).

(G) Nocodazole-arrested HeLa Flp-In T-REx cells that inducibly express LAP-tagged BUBR1-WT or its PP2A-binding mutant (ΔKARD) were treated with control (siControl) or BUBR1 (siBUBR1) siRNAs and stained for T461ph.

(H) Quantification of the T461ph/BUB1 ratio in (G).

(I) EGFP-traps from nocodazole-arrested HeLa cells expressing LAP-tagged BUBR1-WT or BUBR1-ΔKARD were used as a phosphatase source to dephosphorylate BUB1-(437-509) that had been sequentially phosphorylated by CDK2 and MPS1.

Scale bar, 5 μm (A, C, E, and G). In (F) and (H), the data represent mean ± SEM (n = 3, ≥10 cells/condition/experiment). See also Figure S4.

kinase-phosphatase pair (Figures 5A–5C). We will further refer to this phosphorylation pulse as the BUB1-centered biochemical timer (BBT).

We subsequently explored theoretically whether a second pulse of BUB1-T461 phosphorylation can be elicited by a sudden increase in MPS1 activity (Figure 5F). First, after triggering the initial pulse of T461 phosphorylation with MPS1 addition, which is followed by PP2A-B56 recruitment and the dephosphorylation of BUB1-T461 (Figure 5F, red curves), we modeled the effect of adding 50% more MPS1 (Figure 5F, black curves).

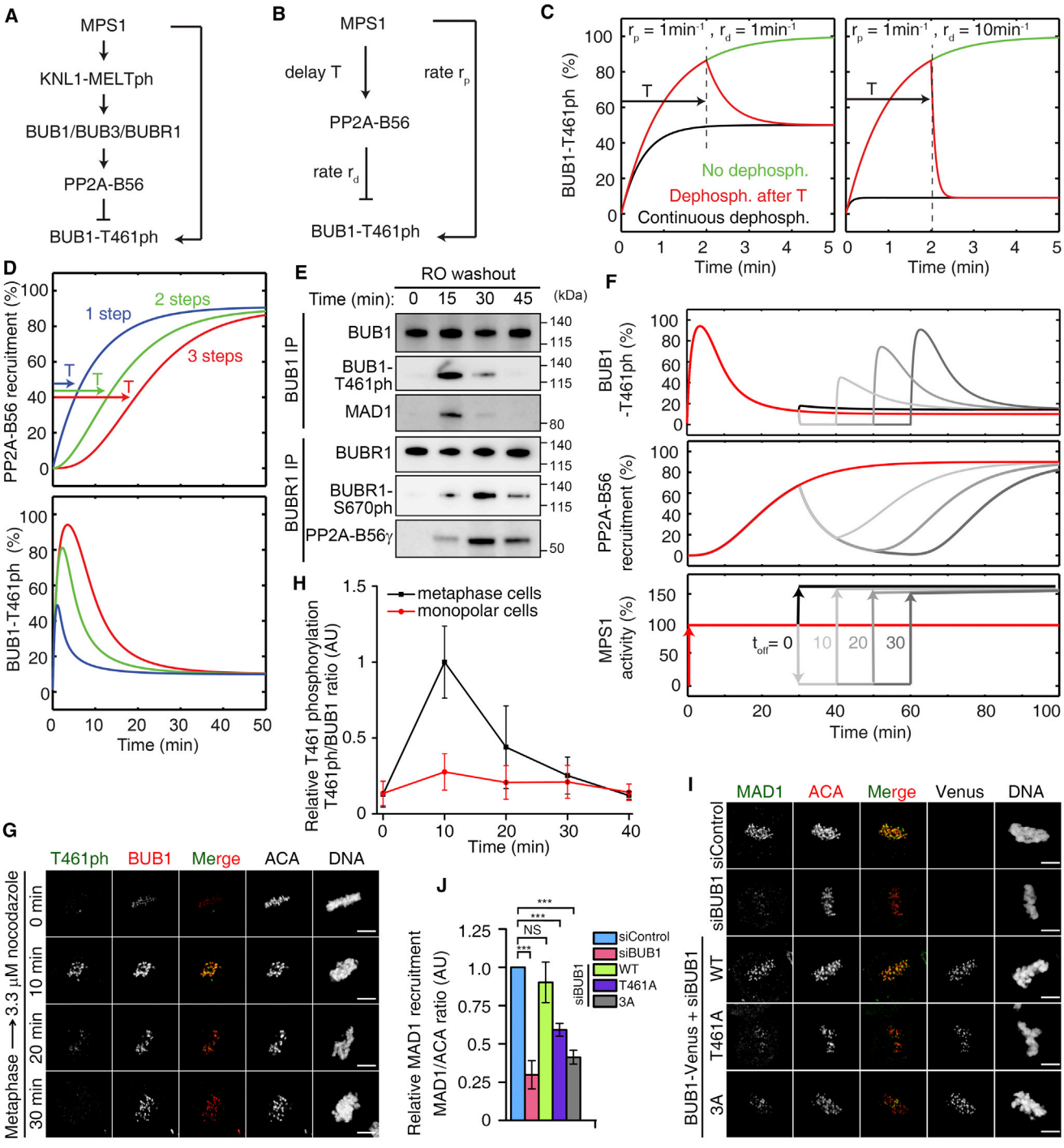

Figure 5. Signaling Profile of the BUB1 Biochemical Timer

(A) Schematic of the components of the BUB1 biochemical timer (BBT) network.

(B) Simplified structure of the BBT, embedded in an incoherent type-1 feedforward loop. r_p, rate of phosphorylation; r_d, rate of dephosphorylation; delay T, time delay associated with phosphatase recruitment.

(C) Simulation of T461 phosphorylation kinetics with different kinase/phosphatase activity ratios. Green curve, only MPS1, no PP2A; red curve, PP2A-B56 is added after MPS1, with time delay (T); black curve, MPS1 and PP2A-B56 are added simultaneously at time 0. Different r_p and r_d values were assigned to the left and right panels.

(D) Simulation of PP2A-B56 activation with a variable number of intermediate steps and corresponding time delays (T) and the resulting T461 phosphorylation kinetics.

(legend continued on next page)

The system response to this stimulus was modest, and a second phosphorylation pulse was not observed. We proceeded to model the effect of removing MPS1 for varying times prior to adding more MPS1. This allows the system to return to its resting state, where all the intermediate substrates, including BUB1-T461, the KNL1 MELT motifs, and the KARD domain of BUBR1, are dephosphorylated (data not shown) and PP2A-B56 is dissociated from the kinetochores (Figure 5F, middle panel, gray curves). The data suggest that the system response to MPS1 addition increases with the duration of the reset time. In other words, there is a refractory period during which the system does not significantly respond to additional MPS1 stimulation.

To experimentally validate these predictions, we used metaphase cells as a model for the reset state, as the end-on MT-KT attachments in metaphase result in the loss of MPS1 and other downstream components from the kinetochores (Hiruma et al., 2015; Ji et al., 2015). However, disruption of end-on MT-KT attachments with nocodazole re-initiated MPS1-kinetochore binding (Figure S5D). Consistent with this finding, the addition of high concentrations of nocodazole to metaphase cells resulted in re-recruitment of BUB1 to the kinetochores and transient BUB1-T461 phosphorylation (Figures 5G and 5H). This biphasic response took approximately 30 min to complete. Intriguingly, when the cells were arrested in a monopolar state using STLC, the addition of an acute dose of nocodazole did not induce transient T461 phosphorylation (Figures 5H and S5E). This is probably a reflection of an incomplete reset state, as lateral MT-KT attachments only moderately reduce MPS1 localization at the kinetochores (Hiruma et al., 2015). In agreement with this interpretation, BUB1 was retained at the kinetochores with STLC treatment (Figure S5E). Indeed, our model predicts that, in these conditions, an increase in MPS1 activity will not induce a robust biphasic response (Figure 5F).

Although BUB1 is dispensable for MAD1 recruitment during prolonged mitosis (Figures 1A and 1B), it is transiently required for MAD1 recruitment when metaphase cells are treated with an acute dose of nocodazole (Vleugel et al., 2015a). This dependency on BUB1 for MAD1 recruitment peaks 10–20 min after nocodazole addition and is lost after 40 min. We speculated that the phosphorylation of BUB1 at T461 and the CDK1-priming sites is required for this transient MAD1 recruitment. Consistent with a previous report (Vleugel et al., 2015a), MAD1 recruitment in metaphase cells treated with nocodazole for 10 min was reduced after BUB1 knockdown (Figures 5I and 5J). MAD1 recruitment was largely restored by the expression of Venus-tagged BUB1-WT, but it was only partially restored by the expression of BUB1-T461A or BUB1-3A. This suggests that BUB1 phosphorylation by MPS1 and CDK1 is required for MAD1 re-recruitment in metaphase.

Importance of the BBT for SAC Signaling

Consistent with the notion that the BBT is not affected by the MT-KT attachment status, a transient phosphorylation of BUB1 at T461 was also observed during mitotic entry after RO3306 release at a concentration of nocodazole (3.3 μM) that completely eliminates microtubule assembly (Figure 6A). Moreover, in these conditions, BUB1 knockdown also prevented MAD1 recruitment in early prometaphase, but not in late or prolonged prometaphase (Figure S6A). Aurora B disrupts erroneous KT-MT interactions and generates unattached kinetochores. We found that the forced targeting of Aurora B to kinetochores by the expression of a MIS12-INCENP-EGFP fusion enhanced the phosphorylation of NDC80 at S55 but did not increase BUB1-T461 phosphorylation in nocodazole-arrested HeLa cells (Figures S6B–S6E), confirming that the BBT functions in an attachment-independent manner.

Next, we sought to delineate the relative importance of the BBT-dependent and attachment-dependent pathways. For MAD1 recruitment and subsequent SAC activation at mitotic entry, several lines of evidence suggest that the BBT pathway responds faster than the attachment-dependent pathway. First, the dependency of MAD1 recruitment on BUB1 peaked at early prometaphase (Figures 1A and 1B). In the absence of BUB1, MAD1 recruitment kept increasing from early prometaphase to late prometaphase, and it peaked in nocodazole-arrested cells (prolonged mitosis with unattached kinetochores). Also, CDC20:MAD2 assembly was delayed in the absence of BUB1 (Figure 2B). Based on these insights, we developed a simple model to simulate the relative contribution of the BBT and attachment-dependent pathways to MAD1 recruitment and APC/C inhibition at mitotic entry. Clearly, when the attachment-dependent pathway is maximally activated (few MT-KT interactions, referred to as high), the BBT is predicted to only make a moderate and transient contribution to overall MAD1 recruitment and APC/C inhibition (Figure 6B, black and red lines). However, when the attachment-dependent pathway is only weakly activated (referred to as intermediate or low), the BBT makes a significant contribution to the initial recruitment of MAD1 and inhibition of the APC/C (Figure 6B, gray lines). Indeed, our simulations suggest that the BBT-dependent pathway may create a safe window at mitotic entry, during

(E) Late G2 HeLa cells were released into fresh medium for the indicated time points, followed by BUB1 or BUBR1 immunoprecipitation, and immunoblot detection.

(F) Simulation of the kinetics of a second biphasic response after completion of the first biphasic response. MPS1 is removed for different durations (T_{off}), after which 150% MPS1 is added.

(G) HeLa cells were synchronized in metaphase by releasing monastrol-arrested cells into MG132 for 2 hr. Cells were subsequently treated with 3.3 μM nocodazole prior to immunostaining for T461ph and BUB1.

(H) Quantification of the T461ph/BUB1 ratio in the nocodazole-treated metaphase cells (release from monastrol arrested to MG132, black curve) or monopolar cells (STLC arrested, red curve). The data represent the mean ± SD (≥10 cells/condition).

(I) HeLa cells expressing Venus-tagged BUB1 WT or the indicated mutants were treated with siRNA and synchronized to metaphase by sequential monastrol-MG132 treatment. Cells were subsequently treated with 3.3 μM nocodazole for 10 min prior to immunostaining.

(J) Quantification of MAD1/ACA ratio in (I). The data represent mean ± SEM (n = 3, ≥10 cells/condition/experiment).

See also Figure S5.

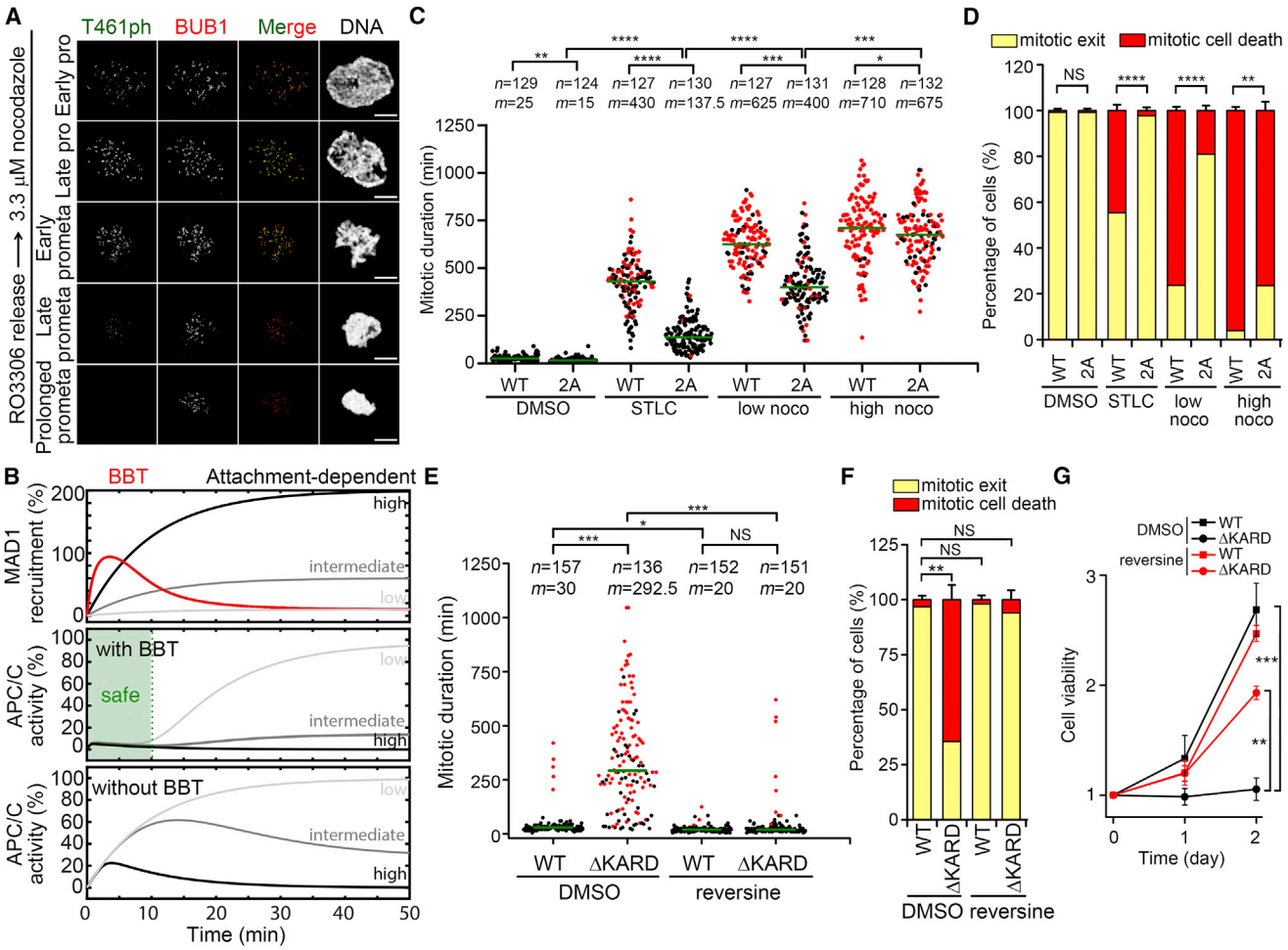

Figure 6. Attachment-Independent Regulation of the BBT and Its Therapeutic Potential

(A) HeLa cells were released from sequential thymidine-RO3306 treatment with 3.3 μM nocodazole for various durations prior to (immuno)staining.

(B) Simulation of APC/C inhibition by the BBT- and attachment-dependent signaling pathways at mitotic entry. The upper panel shows the relative activity of the BBT (red curve) and other attachment-dependent MAD1 recruitment pathways (curves in different shades of gray). The middle and bottom panels show APC/C activation in the presence and absence of the BUB1 pathway, respectively. The green area is denoted as a potential safe window (safe).

(C) Endogenous BUB1 was knocked down in HeLa cells that expressed Venus-tagged BUB1-WT or BUB1-S459A/T461A (2A), which were imaged by DIC time lapse.

(D) Quantification of cell fate in (C). Shown is the mean percentage ± SEM (n = 3).

(E) Endogenous BUBR1 was knocked down in HeLa cells expressing LAP-tagged BUBR1-WT or BUBR1-ΔKARD. Cells were synchronized with thymidine for 24 hr and released into fresh medium for 6 hr prior to drug treatments (DMSO or 500 nM reversine) and DIC time-lapse imaging.

(F) Quantification of cell fate in (E). The graph shows the mean percentage ± SEM (n = 3).

(G) Cell growth in HeLa cells expressing LAP-tagged BUBR1-WT or BUBR1-ΔKARD after knockdown of endogenous BUBR1, as determined by MTT assays. The graph shows the mean percentage ± SEM (n = 3).

In (C) and (E), black dots indicate the duration of mitosis in individual cells, and red dots represent the duration of mitotic cell death. *n*, number of cells; *m*, median duration of mitosis (green line) from three independent experiments. See also Figure S6.

which the APC/C is efficiently inhibited, even if the attachment-dependent pathway is only weakly activated (Figure 6B, middle and lower panels).

To test the modeled scenarios experimentally, we used cell lines that inducibly expressed BUB1-WT, BUB1-S459A/T461A (2A), or BUB1-ΔMAD1 after knockdown of endogenous BUB1. BUB1-2A-expressing cells proceeded through mitosis 10 min faster than BUB1-WT cells (Figure 6C), indicating that the BBT pathway has an important contribution to SAC strength during unperturbed mitosis. The expression of BUB1-2A also considerably reduced the duration of mitosis (Figure 6C) and associated cell death (Figure 6D) in cells that had been treated with STLC or nocodazole to activate attachment-dependent SAC signaling. Importantly, these reductions were more pronounced with STLC and a low concentration of nocodazole than with a high concentration of nocodazole. Hence, the contribution of the BBT to SAC strength decreases with increased levels of unattached kinetochores, in line with the modeling predictions

(Figure 6B). Similar but somewhat stronger effects were obtained with BUB1-ΔMAD1 (Figures S6F and S6G). These data represent functional confirmation for the attachment-independent operation of the BBT.

During interphase, a kinetochore-independent pool of MCC is generated from MAD1:MAD2 dimers that are tethered to nuclear pore complexes (NPCs) (Maciejowski et al., 2010; Meraldi et al., 2004; Rodriguez-Bravo et al., 2014). This pool of interphase MCC was proposed to function as an interphase timer for SAC signaling and APC/C inhibition. To delineate the relative contribution of the NPC timer and BBT to SAC signaling, we used a previously established HCT116 cell line where endogenous MAD1 is replaced by an N-terminal deletion mutant (ΔNP2) (Rodriguez-Bravo et al., 2014). In this cell line, the localization of MAD1 to the nuclear envelope is abolished, which prevents the formation of interphase MCC and shortens mitotic duration. We found that the knockdown of BUB1 in this cell line further shortened the duration of mitosis (Figure S6H), suggesting that the BBT acts in parallel to the NPC-dependent pathway.

Therapeutic Potential of Targeting the BBT

One SAC-directed cancer therapy aims to induce mitotic cell death through chronic SAC activation with microtubule-targeting reagents. However, the clinical use of such reagents is limited by severe side effects, including neurotoxicity. For example, the clinically relevant concentration of Vincristine (VCR) is only about 1 nM (Estlin et al., 2000), which did not efficiently kill cultured HeLa cells (Figures S6I and S6J). Since BUBR1-associated PP2A-B56 silences both BBT signaling (this work) and the recruitment of BUBs to the kinetochores (Espert et al., 2014; Nijenhuis et al., 2014), we examined whether the disruption of BUBR1:PP2A-B56 interaction could chronically activate the SAC and induce cell death. In cells that had endogenous BUBR1 knocked down, the median duration of mitosis amounted to 30 min after the expression of BUBR1-WT but 293 min after the expression of BUBR1-ΔKARD (Figure 6E). This BUBR1-ΔKARD-induced phenotype was rescued by inhibiting MPS1 with reversine, demonstrating that it was caused by chronic SAC activation. Strikingly, 64% of the BUBR1-ΔKARD-expressing cells died during mitosis, which compares to just 3% of the BUBR1-WT-expressing cells (red dots in Figure 6E; Figure 6F). Colorimetric 3-(4,5-dimethylthiazol-2-yl)-2,5-diphenyltetrazolium bromide (MTT) assays demonstrated that BUBR1-ΔKARD expression dramatically reduced global cell proliferation, which was also largely rescued by reversine treatment (Figure 6G). Furthermore, the deadly phenotype in BUBR1-ΔKARD cells was rescued by BUB1 knockdown (Figures S6K and S6L), confirming that the mitotic arrest and cell death in BUBR1-ΔKARD cells is caused, at least in part, by BUB1-dependent chronic SAC activation.

DISCUSSION

In yeast, Bub1 is the sole kinetochore receptor for Mad1 (see the Introduction). It has been more difficult to establish the role of mammalian BUB1 as a MAD1 receptor because of the existence of additional MAD1 receptors. Moreover, as we have shown, mammalian BUB1 only binds transiently to MAD1, and this interaction is lost during prolonged prometaphase arrest. These data at least partly reconcile previous discrepant findings on the contribution of BUB1 to kinetochore recruitment of MAD1 (see the Introduction). *In vitro* reconstitution experiments revealed a direct Bub1:Mad1 interaction in yeast, and this has also been shown for the human orthologs (Faesen et al., 2017; Ji et al., 2017; Zhang et al., 2017). However, the human BUB1:MAD1 interaction was rather weak, suggesting that additional components may be required for stable complex formation. As ZW10 kinetochore localization was only transiently dependent on BUB1, while MAD1 localization was dependent on ZW10 in all tested conditions, this suggests that the RZZ complex somehow stabilizes the BUB1:MAD1 interaction. Consistent with *in vitro* data (Faesen et al., 2017; Ji et al., 2017; Zhang et al., 2017), we found that BUB1 recruits both MAD1 and CDC20 to promote CDC20:C-MAD2 assembly in a cellular context.

BUB1:MAD1 interaction is critically dependent on BUB1-T461 phosphorylation by MPS1. A similar regulation also applies to yeast orthologs. BUB1-T461 is dephosphorylated by the BUBR1-associated pool of PP2A-B56, but this only occurs after a delay because PP2A-B56 kinetochore recruitment requires multiple, time-consuming steps. Delayed PP2A-B56 kinetochore recruitment explains why BUB1 phosphorylation is transient and pulse-like in nature. Another key property of BUB1-T461 dephosphorylation is that it is not affected by MT-KT interactions. As such, the BUB1-T461 phosphorylation pulse functions as a biochemical timer that initiates SAC signaling at mitotic entry regardless of the MT-KT attachment status. The BBT only functions once during normal mitosis and cannot be reactivated during a refractory period. Intriguingly, phosphorylation of BUB1 at S459 by CDK1 is required, but not sufficient, for the induction of the BBT, suggesting that CDK1 serves to license MPS1 to initiate the BBT.

Collectively, our data suggest that the mammalian spindle checkpoint is controlled by both an attachment-independent timer (BBT) and attachment-dependent sensors (Figure 7A). The BBT is activated in multiple steps. During prophase, MPS1 first phosphorylates the MELT repeats of KNL1, enabling the recruitment of BUB proteins, including BUB1 (London et al., 2012; Shepperd et al., 2012; Yamagishi et al., 2012). After phosphorylation of the extended BUB1 CD1 domain by CDK1, MPS1 also phosphorylates BUB1 at T461, which allows the recruitment of MAD1:C-MAD2 in early prometaphase. Finally, MPS1 phosphorylates MAD1 to promote MAD1:CDC20 interaction, which is a key step in the assembly of CDC20:C-MAD2 (Faesen et al., 2017; Ji et al., 2017). Thus, MPS1 guides MCC assembly at three levels, and BUB1 serves as a scaffold for the recruitment of both MAD1 and CDC20. BBT silencing also occurs in a stepwise fashion. Initially, BUBR1 and PP2A-B56 are sequentially recruited to the kinetochores during early prometaphase. This pool of PP2A-B56 dephosphorylates BUB1 at T461, which disrupts the BUB1:MAD1 interaction. BUBR1-associated PP2A-B56 also contributes to the dephosphorylation of the MELT repeats of KNL1 in late prometaphase, either directly or indirectly, by promoting the recruitment of PP1 to KNL1 (Espert et al., 2014; Nijenhuis et al., 2014).

While the BBT pathway of SAC signaling functions as a biochemical timer, the attachment-dependent pathway functions as a sensor that monitors the MT-KT attachment status

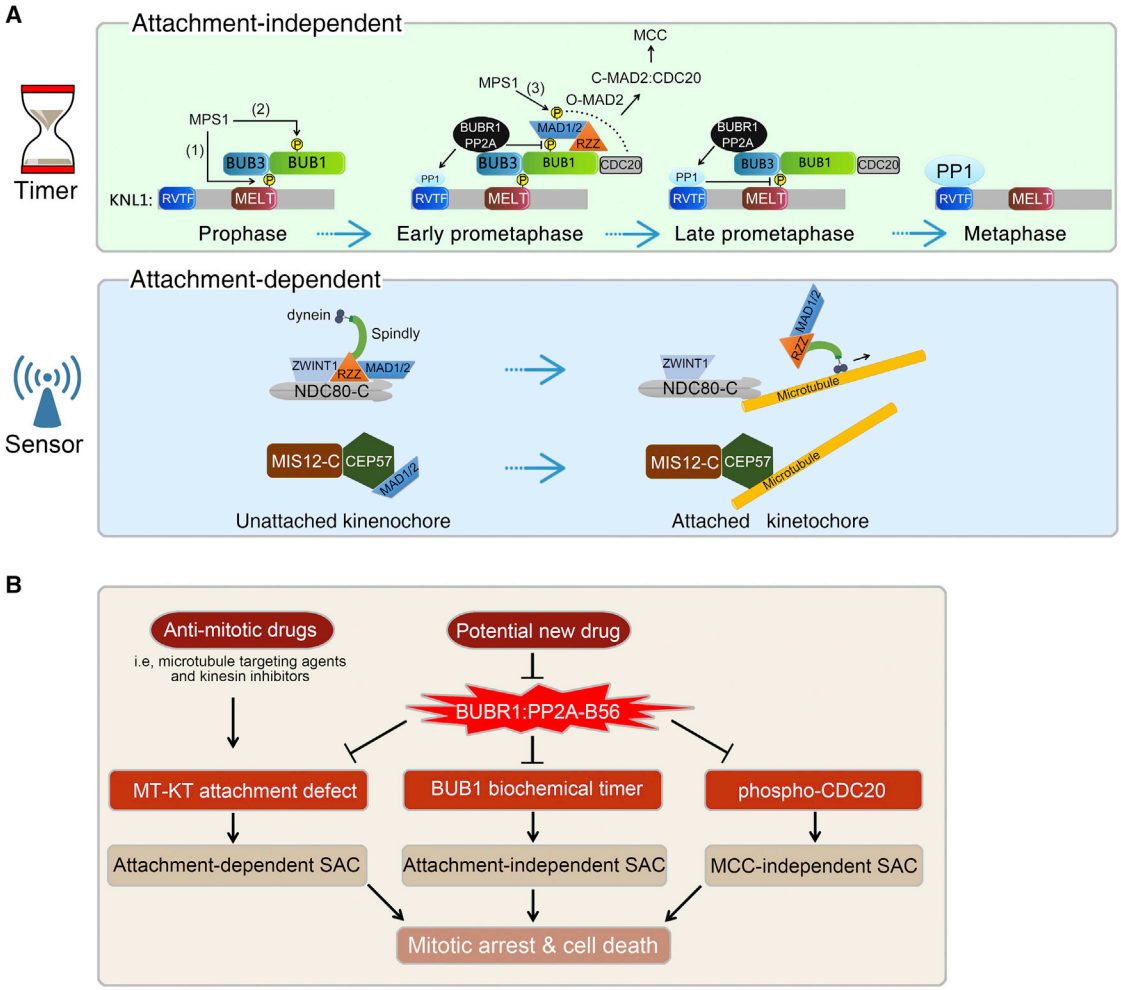

Figure 7. Working Models of the BBT and Attachment-Independent SAC Pathways and Their Therapeutic Potential

(A) Models of MAD1 kinetochore recruitment by the transient BBT-dependent timer pathway (attachment independent) and two potential attachment-dependent sensor pathways. Note that phosphorylation by CDK1 has been omitted for simplification.

(B) Scheme depicting chronic SAC activation as a cancer-killing strategy. Activating multiple SAC pathways by targeting the BUBR1:PP2A-B56 complex is suggested as a therapeutic strategy.

(Figure 7A). Several attachment-sensing mechanisms for the kinetochore dissociation of MAD1 have been described, including Dynein-Spindly-RZZ-mediated stripping of MAD1/2 from the kinetochores and competition between MAD1/2 and microtubules for binding to MIS12-associated CEP57 (Zhou et al., 2016). The existence of both timer and sensor mechanisms for SAC activation raises questions about their specific roles and redundancy. We propose that the BBT creates a safe window during which the SAC is transiently activated and the sensor mechanisms can become fully active. If the SAC is rapidly satisfied, as is probably the case during division of most normal cells, the sensors may not need to be fully activated, and this could be a cellular energy-saving strategy. Strikingly, the BBT lasts for approximately 30 min, which is close to the time that normal human cells require to progress from NEB to anaphase onset (Araujo et al., 2016).

The contribution of the BBT to SAC maintenance drops dramatically in the presence of high levels of unattached kinetochores, confirming that the BBT operates independently of attachment. It also suggests that the sensor pathway dominates SAC maintenance. Nevertheless, the BBT still contributes to SAC signaling during prolonged prometaphase, when the major peak of BUB1-T461 phosphorylation and BUB1-mediated MAD1 recruitment is over. The underlying mechanism is currently unclear and needs further investigation.

MCC generated in interphase by NPC-associated MAD1 controls the speed and fidelity of mitosis (Rodriguez-Bravo et al., 2014), which is similar to the role of the BBT. However, both mechanisms operate at different times. The NPC timer is active in interphase and early mitosis until NEB, while the BBT is activated after NEB. Our simulations suggest that both timers contribute to preventing APC/C activation in early mitosis (Figure S7). Since the NPC timer, BBT, and attachment-dependent sensors suppress APC/C activation in different time windows, we propose that their temporal coordination is essential to

maintaining an effective SAC until correct attachment of the microtubules to the kinetochores is achieved.

Our data suggest that the BBT pathway holds great potential as a target for novel cancer therapies. Clinically used anti-mitotic drugs, such as microtubule-targeting agents, activate the SAC largely via attachment-dependent sensor pathways (Figure 7A). However, disrupting BUBR1:PP2A-B56 also induces massive mitotic cell death through a number of potential mechanisms (Figure 7B). It constitutively activates the BBT pathway but also prevents the dephosphorylation of Aurora B substrates, and thereby it promotes destabilization of MT-KT interactions and activation of attachment-dependent SAC signaling (Foley et al., 2011; Kruse et al., 2013; Suijkerbuijk et al., 2012). Furthermore, in the absence of BUBR1-associated PP2A-B56, CDC20 remains phosphorylated at its PLK1 sites, and this prevents APC/C activation in parallel to MCC assembly (Craney et al., 2016; Jia et al., 2016). Thus, lying at the convergence of three different SAC activation pathways, BUBR1-associated PP2A-B56 appears an attractive target to kill cancer cells in mitosis. Since the BUBR1:PP2A-B56 complex probably only exists during mitosis, its targeting may result in fewer neurotoxic side effects than current anti-mitotic drugs.

In conclusion, we have shown here that the mammalian spindle checkpoint is controlled by a hitherto unrecognized biochemical timer that transiently drives mitotic MCC assembly independently of the MT-KT attachment status. This gives the cells time to initiate attachment-sensing mechanisms that prolong SAC signaling until all chromosomes are properly attached to the kinetochores.

STAR★METHODS

Detailed methods are provided in the online version of this paper and include the following:

- KEY RESOURCES TABLE
- CONTACT FOR REAGENT AND RESOURCE SHARING
- EXPERIMENTAL MODEL AND SUBJECT DETAILS
  - Cell culture
  - Yeast strains and plasmids
- METHOD DETAILS
  - Materials
  - Stable cell line generation and treatment
  - Biochemical procedures
  - Immunofluorescence and microscopy
  - Models of the BUB1 biochemical timer
  - Yeast two hybrid assay
- QUANTIFICATION AND STATISTICAL ANALYSIS
- DATA AND SOFTWARE AVAILABILITY

SUPPLEMENTAL INFORMATION

Supplemental Information includes seven figures and three tables and can be found with this article online at https://doi.org/10.1016/j.molcel.2017.10.011.

AUTHOR CONTRIBUTIONS

J.Q. conceived the project, designed the experiments, and wrote the first version of manuscript. J.Q. performed most of the human cell experiments and analyzed the data. M.A.G.-G., J.C.I., M.H., and P.S. performed the budding yeast experiments and analyzed the data. M. Beullens provided reagents and co-designed the *in vitro* assays. M.G.M. performed the MTT assay. G.V.d.H. performed the *in vitro* (de)phosphorylation assays and quantified the live-cell imaging data. J.Q., M.G.M., and G.V.d.H. generated the stable cell lines. L.G. performed all the simulations and contributed to the writing. M. Bollen co-designed the experiments, coordinated the teams, and revised the manuscript.

ACKNOWLEDGMENTS

This work was supported by the Fund for Scientific Research-Flanders (grant G0B9917N and GOA5317N), a Flemish Concerted Research Action (GOA/15/016), and the Belgian Foundation Against Cancer. We thank Prasad Jallepalli, Geert Kops, Susanne Lens, Jakob Nilsson, Jonathon Pines, Adrian Saurin, Stephen Taylor, and Hongtao Yu for the gift of essential research tools and Bart Lesage for valuable discussions. Madryn Lake is acknowledged for proofreading of the manuscript. Nicole Sente and Annemie Hoogmartens provided expert technical assistance.

Received: March 29, 2017
Revised: August 24, 2017
Accepted: October 11, 2017
Published: November 9, 2017

SUPPORTING CITATIONS

The following references appear in the Supplemental Information: Elowe et al. (2007); Hégarat et al. (2014); Lu et al. (2012); Qian et al. (2011); Qian et al. (2013).

REFERENCES

Araujo, A.R., Gelens, L., Sheriff, R.S.M., and Santos, S.D.M. (2016). Positive Feedback Keeps Duration of Mitosis Temporally Insulated from Upstream Cell-Cycle Events. Mol. Cell *64*, 362–375.

Caldas, G.V., Lynch, T.R., Anderson, R., Afreen, S., Varma, D., and DeLuca, J.G. (2015). The RZZ complex requires the N-terminus of KNL1 to mediate optimal Mad1 kinetochore localization in human cells. Open Biol. *5*, 150160.

Craney, A., Kelly, A., Jia, L., Fedrigo, I., Yu, H., and Rape, M. (2016). Control of APC/C-dependent ubiquitin chain elongation by reversible phosphorylation. Proc. Natl. Acad. Sci. USA *113*, 1540–1545.

Di Fiore, B., Davey, N.E., Hagting, A., Izawa, D., Mansfeld, J., Gibson, T.J., and Pines, J. (2015). The ABBA motif binds APC/C activators and is shared by APC/C substrates and regulators. Dev. Cell *32*, 358–372.

Elowe, S., Hümmer, S., Uldschmid, A., Li, X., and Nigg, E.A. (2007). Tension-sensitive Plk1 phosphorylation on BubR1 regulates the stability of kinetochore microtubule interactions. Genes Dev. *21*, 2205–2219.

Elowe, S., Dulla, K., Uldschmid, A., Li, X., Dou, Z., and Nigg, E.A. (2010). Uncoupling of the spindle-checkpoint and chromosome-congression functions of BubR1. J. Cell Sci. *123*, 84–94.

Espert, A., Uluocak, P., Bastos, R.N., Mangat, D., Graab, P., and Gruneberg, U. (2014). PP2A-B56 opposes Mps1 phosphorylation of Knl1 and thereby promotes spindle assembly checkpoint silencing. J. Cell Biol. *206*, 833–842.

Estlin, E.J., Ronghe, M., Burke, G.A.A., and Yule, S.M. (2000). The clinical and cellular pharmacology of vincristine, corticosteroids, L-asparaginase, anthracyclines and cyclophosphamide in relation to childhood acute lymphoblastic leukaemia. Br. J. Haematol. *110*, 780–790.

Faesen, A.C., Thanasoula, M., Maffini, S., Breit, C., Müller, F., van Gerwen, S., Bange, T., and Musacchio, A. (2017). Basis of catalytic assembly of the mitotic checkpoint complex. Nature *542*, 498–502.

Foley, E.A., Maldonado, M., and Kapoor, T.M. (2011). Formation of stable attachments between kinetochores and microtubules depends on the B56-PP2A phosphatase. Nat. Cell Biol. *13*, 1265–1271.

Hégarat, N., Vesely, C., Vinod, P.K., Ocasio, C., Peter, N., Gannon, J., Oliver, A.W., Novák, B., and Hochegger, H. (2014). PP2A/B55 and Fcp1 regulate Greatwall and Ensa dephosphorylation during mitotic exit. PLoS Genet. *10*, e1004004.

Heinrich, S., Sewart, K., Windecker, H., Langegger, M., Schmidt, N., Hustedt, N., and Hauf, S. (2014). Mad1 contribution to spindle assembly checkpoint signalling goes beyond presenting Mad2 at kinetochores. EMBO Rep. *15*, 291–298.

Hewitt, L., Tighe, A., Santaguida, S., White, A.M., Jones, C.D., Musacchio, A., Green, S., and Taylor, S.S. (2010). Sustained Mps1 activity is required in mitosis to recruit O-Mad2 to the Mad1-C-Mad2 core complex. J. Cell Biol. *190*, 25–34.

Hiruma, Y., Sacristan, C., Pachis, S.T., Adamopoulos, A., Kuijt, T., Ubbink, M., von Castelmur, E., Perrakis, A., and Kops, G.J. (2015). Competition between MPS1 and microtubules at kinetochores regulates spindle checkpoint signaling. Science *348*, 1264–1267.

Ji, Z., Gao, H., and Yu, H. (2015). Kinetochore attachment sensed by competitive Mps1 and microtubule binding to Ndc80C. Science *348*, 1260–1264.

Ji, Z., Gao, H., Jia, L., Li, B., and Yu, H. (2017). A sequential multi-target Mps1 phosphorylation cascade promotes spindle checkpoint signaling. eLife *6*, 1–23.

Jia, L., Li, B., and Yu, H. (2016). The Bub1-Plk1 kinase complex promotes spindle checkpoint signalling through Cdc20 phosphorylation. Nat. Commun. *7*, 10818.

Kim, S., Sun, H., Tomchick, D.R., Yu, H., and Luo, X. (2012). Structure of human Mad1 C-terminal domain reveals its involvement in kinetochore targeting. Proc. Natl. Acad. Sci. USA *109*, 6549–6554.

Klebig, C., Korinth, D., and Meraldi, P. (2009). Bub1 regulates chromosome segregation in a kinetochore-independent manner. J. Cell Biol. *185*, 841–858.

Kops, G.J.P.L., Kim, Y., Weaver, B.A.A., Mao, Y., McLeod, I., Yates, J.R., 3rd, Tagaya, M., and Cleveland, D.W. (2005). ZW10 links mitotic checkpoint signaling to the structural kinetochore. J. Cell Biol. *169*, 49–60.

Kruse, T., Zhang, G., Larsen, M.S.Y., Lischetti, T., Streicher, W., Kragh Nielsen, T., Bjørn, S.P., and Nilsson, J. (2013). Direct binding between BubR1 and B56-PP2A phosphatase complexes regulate mitotic progression. J. Cell Sci. *126*, 1086–1092.

Liu, S.T., Rattner, J.B., Jablonski, S.A., and Yen, T.J. (2006). Mapping the assembly pathways that specify formation of the trilaminar kinetochore plates in human cells. J. Cell Biol. *175*, 41–53.

London, N., and Biggins, S. (2014). Mad1 kinetochore recruitment by Mps1-mediated phosphorylation of Bub1 signals the spindle checkpoint. Genes Dev. *28*, 140–152.

London, N., Ceto, S., Ranish, J.A., and Biggins, S. (2012). Phosphoregulation of Spc105 by Mps1 and PP1 regulates Bub1 localization to kinetochores. Curr. Biol. *22*, 900–906.

Lu, Q., Lu, Z., Liu, Q., Guo, L., Ren, H., Fu, J., Jiang, Q., Clarke, P.R., and Zhang, C. (2012). Chromatin-bound NLS proteins recruit membrane vesicles and nucleoporins for nuclear envelope assembly via importin-α/β. Cell Res. *22*, 1562–1575.

Maciejowski, J., George, K.A., Terret, M.-E.E., Zhang, C., Shokat, K.M., and Jallepalli, P.V. (2010). Mps1 directs the assembly of Cdc20 inhibitory complexes during interphase and mitosis to control M phase timing and spindle checkpoint signaling. J. Cell Biol. *190*, 89–100.

Mangan, S., and Alon, U. (2003). Structure and function of the feed-forward loop network motif. Proc. Natl. Acad. Sci. USA *100*, 11980–11985.

Meraldi, P., Draviam, V.M., and Sorger, P.K. (2004). Timing and checkpoints in the regulation of mitotic progression. Dev. Cell *7*, 45–60.

Musacchio, A. (2015). The Molecular Biology of Spindle Assembly Checkpoint Signaling Dynamics. Curr. Biol. *25*, R1002–R1018.

Nijenhuis, W., Vallardi, G., Teixeira, A., Kops, G.J.P.L., and Saurin, A.T. (2014). Negative feedback at kinetochores underlies a responsive spindle checkpoint signal. Nat. Cell Biol. *16*, 1257–1264.

Qi, W., and Yu, H. (2007). KEN-box-dependent degradation of the Bub1 spindle checkpoint kinase by the anaphase-promoting complex/cyclosome. J. Biol. Chem. *282*, 3672–3679.

Qian, J., Lesage, B., Beullens, M., Van Eynde, A., and Bollen, M. (2011). PP1/Repo-man dephosphorylates mitotic histone H3 at T3 and regulates chromosomal aurora B targeting. Curr. Biol. *21*, 766–773.

Qian, J., Beullens, M., Lesage, B., and Bollen, M. (2013). Aurora B defines its own chromosomal targeting by opposing the recruitment of the phosphatase scaffold Repo-Man. Curr. Biol. *23*, 1136–1143.

Qian, J., Beullens, M., Huang, J., De Munter, S., Lesage, B., and Bollen, M. (2015). Cdk1 orders mitotic events through coordination of a chromosome-associated phosphatase switch. Nat. Commun. *6*, 10215.

Rodriguez-Bravo, V., Maciejowski, J., Corona, J., Buch, H.K., Collin, P., Kanemaki, M.T., Shah, J.V., and Jallepalli, P.V. (2014). Nuclear pores protect genome integrity by assembling a premitotic and Mad1-dependent anaphase inhibitor. Cell *156*, 1017–1031.

Rosenberg, J.S., Cross, F.R., and Funabiki, H. (2011). KNL1/Spc105 recruits PP1 to silence the spindle assembly checkpoint. Curr. Biol. *21*, 942–947.

Schaaff, I., Green, J.B.A., Gozalbo, D., and Hohmann, S. (1989). A deletion of the PDC1 gene for pyruvate decarboxylase of yeast causes a different phenotype than previously isolated point mutations. Curr. Genet. *15*, 75–81.

Shepperd, L.A., Meadows, J.C., Sochaj, A.M., Lancaster, T.C., Zou, J., Buttrick, G.J., Rappsilber, J., Hardwick, K.G., and Millar, J.B.A. (2012). Phosphodependent recruitment of Bub1 and Bub3 to Spc7/KNL1 by Mph1 kinase maintains the spindle checkpoint. Curr. Biol. *22*, 891–899.

Silió, V., McAinsh, A.D., and Millar, J.B. (2015). KNL1-Bubs and RZZ Provide Two Separable Pathways for Checkpoint Activation at Human Kinetochores. Dev. Cell *35*, 600–613.

Suijkerbuijk, S.J.E., Vleugel, M., Teixeira, A., and Kops, G.J.P.L. (2012). Integration of kinase and phosphatase activities by BUBR1 ensures formation of stable kinetochore-microtubule attachments. Dev. Cell *23*, 745–755.

Taylor, S.S., and McKeon, F. (1997). Kinetochore localization of murine Bub1 is required for normal mitotic timing and checkpoint response to spindle damage. Cell *89*, 727–735.

Van Dessel, N., Beke, L., Görnemann, J., Minnebo, N., Beullens, M., Tanuma, N., Shima, H., Van Eynde, A., and Bollen, M. (2010). The phosphatase interactor NIPP1 regulates the occupancy of the histone methyltransferase EZH2 at Polycomb targets. Nucleic Acids Res. *38*, 7500–7512.

van Meerloo, J., Kaspers, G.J.L., and Cloos, J. (2011). Cell sensitivity assays: the MTT assay. Methods Mol. Biol. *731*, 237–245.

Vleugel, M., Tromer, E., Omerzu, M., Groenewold, V., Nijenhuis, W., Snel, B., and Kops, G.J.P.L. (2013). Arrayed BUB recruitment modules in the kinetochore scaffold KNL1 promote accurate chromosome segregation. J. Cell Biol. *203*, 943–955.

Vleugel, M., Hoek, T.A., Tromer, E., Sliedrecht, T., Groenewold, V., Omerzu, M., and Kops, G.J.P.L. (2015a). Dissecting the roles of human BUB1 in the spindle assembly checkpoint. J. Cell Sci. *128*, 2975–2982.

Vleugel, M., Omerzu, M., Groenewold, V., Hadders, M.A., Lens, S.M.A., and Kops, G.J.P.L. (2015b). Sequential multisite phospho-regulation of KNL1-BUB3 interfaces at mitotic kinetochores. Mol. Cell *57*, 824–835.

Yamagishi, Y., Yang, C.-H., Tanno, Y., and Watanabe, Y. (2012). MPS1/Mph1 phosphorylates the kinetochore protein KNL1/Spc7 to recruit SAC components. Nat. Cell Biol. *14*, 746–752.

Yang, X., Hubbard, E.J., and Carlson, M. (1992). A protein kinase substrate identified by the two-hybrid system. Science *257*, 680–682.

Zhang, G., Lischetti, T., Hayward, D.G., and Nilsson, J. (2015). Distinct domains in Bub1 localize RZZ and BubR1 to kinetochores to regulate the checkpoint. Nat. Commun. *6*, 7162.

Zhang, G., Kruse, T., López-Méndez, B., Sylvestersen, K.B., Garvanska, D.H., Schopper, S., Nielsen, M.L., and Nilsson, J. (2017). Bub1 positions Mad1 close to KNL1 MELT repeats to promote checkpoint signalling. Nat. Commun. *8*, 15822.

Zhou, H., Wang, T., Zheng, T., Teng, J., and Chen, J. (2016). Cep57 is a Mis12-interacting kinetochore protein involved in kinetochore targeting of Mad1-Mad2. Nat. Commun. *7*, 10151.

STAR★METHODS

KEY RESOURCES TABLE

REAGENT or RESOURCE	SOURCE	IDENTIFIER
Antibodies		
Rabbit anti-GFP	Santa Cruz	Cat# sc-8334; RRID:AB_641123
Mouse anti-GFP	Santa Cruz	Cat# sc-9996; RRID:AB_627695
Rabbit anti-GAPDH	Cell Signaling	Cat# 2118; RRID:AB_561053
Mouse anti-BUB1	Abcam	Cat# ab54893; RRID:AB_940664
Rabbit anti-BUBR1	Bethyl Laboratories	Cat# A300-386A; RRID:AB_386097
Mouse anti-BUBR1	Santa Cruz	Cat# sc-47744; RRID:AB_781706
Mouse anti-CDC20	Santa Cruz	Cat# sc-5296; RRID:AB_628090
Mouse anti-H3S10ph	Cell Signaling	Cat# 9706; RRID:AB_331748
Human anti-ACA	ImmunoVision	Cat# HCT-0100
Rabbit anti-MAD1	Santa Cruz	Cat# sc-67338; RRID:AB_2139257
Mouse anti-MAD1	Santa Cruz	Cat# sc-47746; RRID:AB_627901
Goat anti-MAD2	Santa Cruz	Cat# sc-6329; RRID:AB_648599
Rabbit anti-ZW10	Abcam	Cat# ab21582; RRID:AB_779030
Mouse anti-PP2A-C	BD Transduction Laboratories	Cat# 610556; RRID:AB_397910
Mouse anti-PP2A-B55	Santa Cruz	Cat# sc-365282; RRID:AB_10843242
Mouse anti-PP2A-B56α	BD Transduction Laboratories	Cat# 610615; RRID:AB_397947
Mouse anti-PP2A-B56γ	Santa Cruz	Cat# sc-67038; RRID:AB_2170434
Mouse anti-cyclin B1	BD Transduction Laboratories	Cat# 554177; RRID:AB_395288
Mouse anti-phospho-Thr-Pro	Cell Signaling	Cat# 9391S; RRID:AB_331801
Rabbit anti-phospho-NDC80-S55	GeneTex	Cat# GTX70017; RRID:AB_11162004
Rabbit anti-phospho-BUBR1-S670	Nijenhuis et al., 2014	N/A
Rabbit anti-phospho-MELT KNL1	Vleugel et al., 2015b	N/A
Mouse anti-non-isoform-specific PP1	Van Dessel et al., 2010	N/A
Rabbit anti-phospho-BUB1-T461	This paper	N/A
Chemicals, Peptides, and Recombinant Proteins		
Calyculin A	Biomol	Cat# EI-192
RO3306	Tocris	Cat# 4181
monastrol	Biorbyt	Cat# orb146117
microcystin-LR	Cayman	Cat# 10007188
nocodazole	Sigma Aldrich	Cat# M1404
STLC (S-trityl-L-cysteine)	Calbiochem	Cat# 324621
MG132	Selleckchem	Cat# S2619
Paclitaxel	LC Laboratories	Cat# P-9600
Deposited Data		
Raw images	This paper	https://doi.org/10.17632/mdkxkdk7x6.1
Experimental Models: Cell Lines		
HeLa	ATCC	ATCC:CCL-2
RPE-1	Dr. Susanne Lens	ATCC:CRL-4000
HEK293T	ATCC	ATCC:CRL-11268
Flp-in T-Rex HeLa	Dr. Jonathon Pines and Dr. Stephen Taylor	N/A

(*Continued on next page*)

Continued

REAGENT or RESOURCE	SOURCE	IDENTIFIER
Flp-In T-REx HeLa expressing BUB1-Venus or its mutants	This paper	N/A
Flp-In T-REx HeLa expressing BUB1-mClover or its mutants	This paper	N/A
Flp-In T-REx HeLa expressing LAP-BUBR1 WT or LAP-BUBR1 and ΔKARD mutant	Nijenhuis et al., 2014	N/A
HCT116 MAD1L1-null cell lines reconstituted with MAD1-WT or the MAD1-ΔNP2 mutant	Rodriguez-Bravo et al., 2014	N/A
Experimental Models: Organisms/Strains		
S. cerevisiae: Strain background: CTY10-5d	Dr. R. Sternglantz	N/A
S. cerevisiae: Strain background: M5α	Schaaff et al., 1989	N/A
Yeast strains, see Table S2	N/A	N/A
Oligonucleotides		
siRNA oligos, see Table S1	N/A	N/A
Recombinant DNA		
BUB1 siRNA-resistant pCDNA5-FRT-BUB1-Venus	Zhang et al., 2015	N/A
BUB1 siRNA-resistant pCDNA5-FRT-BUB1-Venus mutants	This paper	N/A
BUB1 siRNA-resistant pCDNA5-FRT-BUB1-mClover and its mutants	This paper	N/A
EGFP-BUB1(437-509)	This paper	N/A
pET16-His-MAD1(597-718)	This Paper	N/A
Plasmids used in *S. cerevisiae*, see Table S3	N/A	N/A
Software and Algorithms		
Fiji 1.51n	https://fiji.sc/	N/A
Photoshop CC	Adobe	N/A
ImageQuant LAS4000 imaging system	GE Healthcare	N/A
Typhoon FLA 9500 system	GE Healthcare	N/A
Origin 8.5	OriginLab software	N/A

CONTACT FOR REAGENT AND RESOURCE SHARING

Requests for resources and reagents should be directed to the Lead Contact, Mathieu Bollen (mathieu.bollen@kuleuven.be).

EXPERIMENTAL MODEL AND SUBJECT DETAILS

Cell culture

HEK293T cells were cultured in high-glucose DMEM supplemented with 10% fetal calf serum (FCS). HeLa cells were cultured in low-glucose DMEM, supplemented with 10% FCS. Flp-In T-REx HeLa host cell lines were routinely maintained in DMEM supplemented with 10% tetracycline-free FCS and 50 μg/mL Zeocin. All media contained penicillin and streptomycin. Flp-In T-REx HeLa cells, used for generating stable doxycycline-inducible Venus-tagged or mClover-tagged BUB1 cell lines, were a gift from Dr. Jonathon Pines (University of Cambridge, UK) and Dr. Stephen Taylor (Manchester University, UK), respectively (Hewitt et al., 2010). Flp-In T-REx HeLa cells expressing LAP-BUBR1 WT and LAP-BUBR1 ΔKARD mutant were a gift from Dr. Adrian Saurin (University of Dundee, UK) (Nijenhuis et al., 2014). HCT116 *MAD1L1*-null cell lines reconstituted with MAD1-WT or the MAD1-ΔNP2 mutant were a gift from Dr. Prasad Jallepalli (Memorial Sloan Kettering Cancer Center, USA). RPE-1 cell line was a gift from Dr. Susanne Lens (University Medical Center Utrecht, Netherlands).

Yeast strains and plasmids

The *S. cerevisiae* strains used in this study are listed in Table S2. Standard genetic analysis and transformation methods were used. To maintain selection for plasmids, yeast cultures were grown in synthetic complete (SC) medium lacking appropriate supplements. Apart from the CTY10-5d stain, all strains were isogenic with the M5α background. Where indicated, strains were generated using plasmid shuffling and FOA (5-fluoorotic acid). Plasmids used in this work are listed in Table S3.

METHOD DETAILS

Materials

Antibodies specific for GFP (sc-8334 and sc-9996, Santa Cruz, 1:1000 for WB; ab6673, Abcam, 1:2000 for WB), GAPDH (2118, Cell Signaling, 1:5000 for WB), BUB1 (ab54893, Abcam, 1:1000 for IF, 1:2000 for WB, 1:100 for IP), BUBR1 (A300-386A, Bethyl Laboratories, 1:1000 for WB; sc-47744, Santa Cruz, 1:100 for IF), CDC20 (sc-5296, Santa Cruz, 1:1000 for IF, 1:2000 for WB, 1:200 for IP), H3S10ph (9706, Cell Signaling, 1:5000 for IF), ACA (anti-centromere antibody, HCT-0100, ImmunoVision, 1:4000 for IF), MAD1 (sc-47746 or sc-67338, Santa Cruz, 1:100 and 1:1000 for IF, respectively), MAD2 (sc-6329, 1:1000 for WB), ZW10 (ab21582, Abcam, 1:1000 for IF), PP2A-C (610556, BD Transduction Laboratories, 1:2000 for WB), PP2A-B55 (sc-365282, Santa Cruz, 1:500 for WB), PP2A-B56α (610615, BD Transduction Laboratories, 1:500 for WB), PP2A-B56γ (sc-67038, Santa Cruz, 1:1000 for WB), cyclin B1 (554177, BD Pharmingen, 1:2000 for WB), NDC80-S55ph (GTX70017,GeneTex, 1:300 for IF), phospho-Thr-Pro (9391, Cell Signaling, 1:1000 for WB) were used in this study. The anti-phospho-MELT KNL1 and BUBR1-S670ph antibodies were a kind gift from Geert Kops (Hubrecht Institute, Netherlands)(Nijenhuis et al., 2014; Vleugel et al., 2015b). A non-isoform-specific monoclonal PP1 antibody was generated as previously described (Van Dessel et al., 2010), and a phospho (ph)-BUB1-T461 specific antibody was generated by coupling the synthetic peptide RRKRKVQSPpTVHTKEAC to keyhole limpet hemocyanin (KLH) and BSA (Imject Maleimide-activated KLH/BSA kit, Pierce). The KLH-coupled phospho-peptide was injected in a rabbit and antigen-specific antibodies were affinity column purified using the BSA-coupled non-phospho-BUB1 peptide before immunostaining. The BUB1-S459ph antibody was a gift from Hongtao Yu (University of Texas Southwestern Medical Center, USA) (Ji et al., 2017) and was further purified using BSA-coupled non-phospho-BUB1 peptide. Secondary antibodies used include swine anti-rabbit IgG-HRP (P0217, Dako, 1:5000), rabbit anti-mouse IgG-HRP (P0260, Dako,1:5000), rabbit anti-goat IgG-HRP (P0160, Dako,1:5000), donkey anti-mouse and goat anti-rabbit IgG-Alexa Fluor® 488 antibodies (A11008 and ab150109 from Invitrogen,1:1000), goat anti-mouse and goat anti-rabbit IgG-Alexa Fluor® 546 antibodies (A11030 and A11010 from Invitrogen,1:1000) and goat anti-mouse, goat anti-rabbit, and goat anti-human IgG-Alexa Fluor® 633 antibodies (A21052, A21070, and A21091 from Invitrogen,1:1000). Treatments included Calyculin A (EI-192, Biomol, 20 nM), RO3306 (4181, Tocris, 9 μM), monastrol (orb146117, Biorbyt, 100 μM), microcystin-LR (10007188, Cayman, 0.5 μM), nocodazole (M1404, Sigma Aldrich, 330 nM for low, 3.3 μM for high), STLC (S-trityl-L-cysteine, 324621, Calbiochem, 7.5 μM), MG132 (S2619, Selleckchem, 10 μM) and taxol (Paclitaxel, P-9600, LC Laboratories, 10 nM for live imaging, 30 nM for immunoblotting). siRNA duplexes were listed in Table S1. Mutants were generated using the QuickChange Mutagenesis Kit (Agilent Technologies) and verified by sequencing. The BUB1 siRNA-resistant pCDNA5-FRT-BUB1-Venus construct was a kind gift from Dr Jakob Nilsson (University of Copenhagen, Denmark) (Zhang et al., 2015).

Stable cell line generation and treatment

HeLa Flp-In T-REx cells that stably express doxycycline-inducible BUB1-Venus or BUB1-mClover were generated by transfecting the HeLa Flp-In host cell line with the pCDNA5/FRT/TO and pOG44 (Invitrogen) vectors, and the culture medium was supplemented with 200 μg/mL hygromycin and 4 μg/mL blasticidin. Gene expression was induced with 100 ng/mL doxycycline (Sigma-Aldrich) for a minimum of 24 h, or as indicated. For RO3306 washout experiments, cells were initially treated with 2 mM thymidine for 24 h, washed twice with PBS, and released in fresh medium for 4 h prior to treatment with 9 μM RO3306. After 8 h, the cells were washed twice with PBS and incubated with fresh medium. Plasmid DNA transfection was performed using X-tremeGENE 9 (Roche Applied Science) or jetPRIME (Polyplus Transfection) transfection reagents. siRNA transfections were performed using Lipofectamine® RNAiMax transfection reagent for 48-60 h.

Biochemical procedures

For EGFP-traps and immunoprecipitations, the soluble fraction (S1) after cell lysis and the chromatin-enriched fraction (S2) after micrococcal nuclease (300 U/mL) treatment were collected as previously described (Qian et al., 2015). The pellet that remained after micrococcal nuclease S2 extraction was sonicated in ice water for 10 min, and the supernatant (S3) was combined with S1 and S2 for EGFP-trapping or antibody pull-down. In fractionation assays (Figure S3I), S1 was considered as cytosolic fraction and S2+S3 was considered as chromosomal fraction. EGFP antibody sc-9996 was used as control mouse IgG for CDC20 IP. For Coomassie brilliant blue staining and immunoblotting, SDS-PAGE was performed with 4%–12% Bis-Tris or 3%–8% Tris-acetate gels (NuPAGE®, Invitrogen). Poly-His-tagged Bub1 fragments from budding yeast were expressed in bacteria and purified on Ni^{2+}-Sepharose. For *in vitro* phosphorylation, purified human EGFP-BUB1-(437-509) traps were incubated for 60 min at 30°C with bacterially expressed and purified His-tagged MPS1-(519-808) and/or CDK2/cyclin A in buffer containing 20 mM Tris/HCl at pH 7.5, 1 mM DTT, 0.1 mg/mL BSA, 2 mM MgAc, 1 mM ATP (γ^{32}P-labeled ATP was added for autoradiography detection). Immunoblots were visualized using ECL reagents (Perkin Elmer) and the ImageQuant LAS4000 imaging system (GE Healthcare). Coomassie brilliant-blue stained radioactive gels were visualized with the Typhoon FLA 9500 system (GE Healthcare). Cell proliferation was measured with the 3-(4,5-dimethylthiazol-2-yl)-2,5-diphenyltetrazolium bromide (MTT) colorimetric assay, which quantifies metabolic activity (van Meerloo et al., 2011).

Immunofluorescence and microscopy

For immunofluorescence studies, cells were grown on polylysine-coated coverslips in 24-well chambers. After a 1 min pre-extraction with CSK buffer (10 mM PIPES at pH 6.8, 100 mM NaCl, 300 mM sucrose, 0.25% Triton X-100, 1 mM

EGTA, 1 mM $MgCl_2$, 20 mM NaF, 20 mM β-glycerophosphate, 0.5 μM Microcystin), cells were fixed with 4% paraformaldehyde, permeabilized with 0.5% Triton X-100 and blocked in 3% BSA/PBS. Cells were subsequently incubated with primary antibodies in 1.5% BSA/PBS overnight at 4°C, and with secondary antibodies for 1 h at room temperature. DNA was stained with DAPI. Confocal images were acquired with a Leica TCS SPE laser-scanning confocal system mounted on a Leica DMI 4000B microscope, and equipped with a Leica ACS APO 63X 1.30NA oil DIC objective. For live cell imaging, the Leica TCS SPE microscope was equipped with a live-imaging chamber (37°C, 5% CO_2), a monochrome DFC365 FX Leica digital camera and a 20 × DIC objective. Identical illumination settings were used to capture immunofluorescence images of similarly stained experiments. Brightness and contrast were adjusted using linear operations, and were applied to the whole image. Final images were processed and assembled using Photoshop® CC (Adobe). For quantification, Z stack scans were performed through each cell (4-6 sections, 0.5 μm intervals), and analyzed using ImageJ software and the Z project 'sum slices' feature. Kinetochore regions were selected manually (for at least 10 kinetochores/cell), based upon the localization of the reference proteins, i.e., ACA or BUB1, or semi-automatically using the threshold-based Macro in ImageJ as previously described (Nijenhuis et al., 2014). The background signal was subtracted prior to calculation of the relative kinetochore signal ratio (protein of interest/reference protein). The normalized ratio was plotted using Origin 8.5 (OriginLab software).

Models of the BUB1 biochemical timer

Initially, we used the simplest possible system to create a biochemical timer from an underlying incoherent feedforward loop, and we included just three parameters (illustrated in Figure 5B): a kinase (MPS1) that phosphorylates the substrate (S; BUB1-T461ph) at rate r_p, a phosphatase (PP2A-B56) that dephosphorylates the substrate at rate r_d, and a discrete time delay (T) in initiating dephosphorylation. These basic interactions were modeled using the following ordinary differential equation (ODE) equation, which we solved using the built in ode23 function in MATLAB:

$$\frac{dS}{dt} = r_p(1 - S) - r_d H(t - T)S$$

where H is a Heaviside step function, which is zero for t < T and one for t > T. Figure 5C shows simulation results using T = 0, 2 min, r_p = 1 min^{-1} and r_d = 1,10 min^{-1}.

We proceeded to use a simple multi-step system to generate a time delay (T) in a biologically more relevant setting. We implemented a phosphorylation cascade where each substrate aids in the phosphorylation of the next substrate, leading to the phosphorylation of the final substrate of interest (PP), which is the phosphatase that can dephosphorylate the substrate (S). We chose either a 1-step, 2-step, or 3-step process, such that the system is now described by the following sets of ODE equations:

1 step:

$$\frac{dPP}{dt} = r_{p1}(1 - PP) - r_{d1}PP$$
$$\frac{dS}{dt} = r_{p2}(1 - S) - r_{d2}PP\,S$$

2 steps:

$$\frac{dK_1}{dt} = r_{p1}(1 - K_1) - r_{d1}K_1$$
$$\frac{dPP}{dt} = r_{p1}K_1(1 - PP) - r_{d1}PP$$
$$\frac{dS}{dt} = r_{p2}(1 - S) - r_{d2}PP\,S$$

3 steps:

$$\frac{dK_1}{dt} = r_{p1}n(1 - K_1) - r_{d1}K_1$$
$$\frac{dK_2}{dt} = r_{p1}K_1(1 - K_2) - r_{d1}K_2$$
$$\frac{dPP}{dt} = r_{p1}K_2(1 - PP) - r_{d1}PP$$
$$\frac{dS}{dt} = r_{p2}n(1 - S) - r_{d2}PP\,S$$

Using MATLAB, we simulated the time evolution of these equations using a custom-written, simple Euler method and the following parameter set: r_{p1} = 0.1 min^{-1}, r_{p2} = 1 min^{-1}, r_{d1} = 0.01 min^{-1}, r_{d2} = 10 min^{-1}, n = 1. All substrates were initially assumed to be dephosphorylated. The results, shown in Figure 5D, illustrate that a longer cascade generates a longer time delay in phosphatase activation, and also a higher-amplitude pulse.

Using the 3-step model, we tested whether another pulse could be triggered by increasing MPS1 activity by 50%. This was achieved by increasing factor n from 1 to 1.5 at time t = 30 min. As shown in Figure 5F (black line), this had a minimal effect on substrate (BUB1-T461) phosphorylation, and produced only a slight transient increase. This was because PP2A-B56 (PP in the model) and the intermediate effectors were still activated or phosphorylated, respectively. We proceeded to introduce a window of varying length (10, 20, or 30 min) during which MPS1 activity was turned off (n = 0), before increasing MPS1 activity (n = 1.5). During this window, the dephosphorylation rate (r_{d1}) was increased to 0.2 min^{-1}. As shown in Figure 5E, when the window is sufficiently long, further pulses of BUB1-T461 phosphorylation can be triggered.

Next, we expanded the model to include qualitative APC/C interaction. The APC/C activity level is determined not only by activation of the substrate (S; BUB1-T461), but also by other MT-KT attachment-dependent MAD1 recruitment mechanisms. When the Hill factor (p) is high (here chosen as p = 10), the steady-state APC/C level is close to 1 (fully active) when the combined effect of MAD1 recruitment and the biochemical timer (S) is small: R + S < 0.5. In contrast, APC/C activity is suppressed (APC = 0) when R + S > 0.5. The speed with which the system approaches this steady state, that is the speed of APC/C activation, is given by the parameter v (here chosen as v = 0.1 min^{-1}). We assume that MAD1 is gradually recruited after NEB, and that the accumulation rate is slower than the response of the BUB1 biochemical timer. The accumulation rate (R) is given by k_a, which we have varied from 0.01 min^{-1} (low) to 0.06 min^{-1} (intermediate) or to 0.2 min^{-1} (high). The MAD1 removal rate (k_i) is taken to be 0.1 min^{-1}, such that the steady-state level of fully recruited MAD1 (R_{SS}) is k_a/k_i. This simple model has been used to illustrate how differences in timescales between the BUB1 biochemical timer and MT-KT attachment-dependent MAD1 recruitment can affect APC/C activation upon mitotic entry. The corresponding ODE equations are shown below, and simulation results, in the presence and absence of the BUB1 biochemical timer, are plotted in Figure 6B. The simulations illustrate that, when the activation of MT-KT attachment-dependent MAD1 recruitment is slow, a relatively fast BUB1 biochemical timer is crucial in maintaining low APC/C activity, thereby allowing MAD1 to accumulate and overcome APC/C suppression via the SAC.

$$\frac{dK_1}{dt} = r_{p1} n (1 - K_1) - r_{d1} K_1$$

$$\frac{dK_2}{dt} = r_{p1} K_1 (1 - K_2) - r_{d1} K_2$$

$$\frac{dPP}{dt} = r_{p1} K_2 (1 - PP) - r_{d1} PP$$

$$\frac{dS}{dt} = r_{p2} n (1 - S) - r_{d2} PP\, S$$

$$\frac{dR}{dt} = k_a - k_i R$$

$$\frac{dAPC}{dt} = \mathrm{v}\left(\frac{1}{1 + (0.5 + R + S)^p} - APC\right)$$

Finally, we explored the potential role of a timer involving nuclear-pore-complex (NPC) associated MAD1, referred to as the NPC timer (Rodriguez-Bravo et al., 2014). We simulated its effect similarly as the attachment-dependent mechanism (R), but as this NPC timer is active in interphase and early mitosis until NEB, we initialized R at a higher level of activity (R = 0.7) such that it is already able to suppress APC/C activation. After NEB, the NPC timer is then gradually deactivated (k_a = 0 min^{-1}, k_i = 1 min^{-1}). The resulting NPC timer is shown in Figure S7 (green), and its effect on APC/C activity is explored for two different values of the APC/C activation rate (v = 0.1, 10 min^{-1}).

Yeast two hybrid assay

The CTY10.5d yeast strain was co-transformed with a plasmid expressing a fusion between Mad1 and the lexA DNA-binding domain (pBTM-*MAD1*), and a plasmid expressing Bub1 (wild-type or derived mutants) fused to the Gal4 activation domain (pGADT7-*BUB1*, pGADT7-*BUB1-S451A*, pGADT7-*BUB1-T453A*, pGADT7-*BUB1-S451E* or pGADT7-*BUB1-T453E*). Yeast transformants were grown on selective plates and were screened for β-galactosidase activity using a filter lift assay (Yang et al., 1992).

QUANTIFICATION AND STATISTICAL ANALYSIS

For all statistical analyses with a *p* value, unpaired Students' t test was used. NS: not significant, *p < 0.05, **p < 0.01, ***p < 0.001, ****p < 0.0001. Error bars represents standard error of the mean (SEM) or standard deviation (SD), as indicated in the legends.

DATA AND SOFTWARE AVAILABILITY

The raw data files for images are available at Mendeley (https://doi.org/10.17632/mdkxkdk7x6.1).

Molecular Cell, Volume *68*

Supplemental Information

An Attachment-Independent Biochemical Timer of the Spindle Assembly Checkpoint

Junbin Qian, Maria Adelaida García-Gimeno, Monique Beullens, Maria Giulia Manzione, Gerd Van der Hoeven, Juan Carlos Igual, Miguel Heredia, Pascual Sanz, Lendert Gelens, and Mathieu Bollen

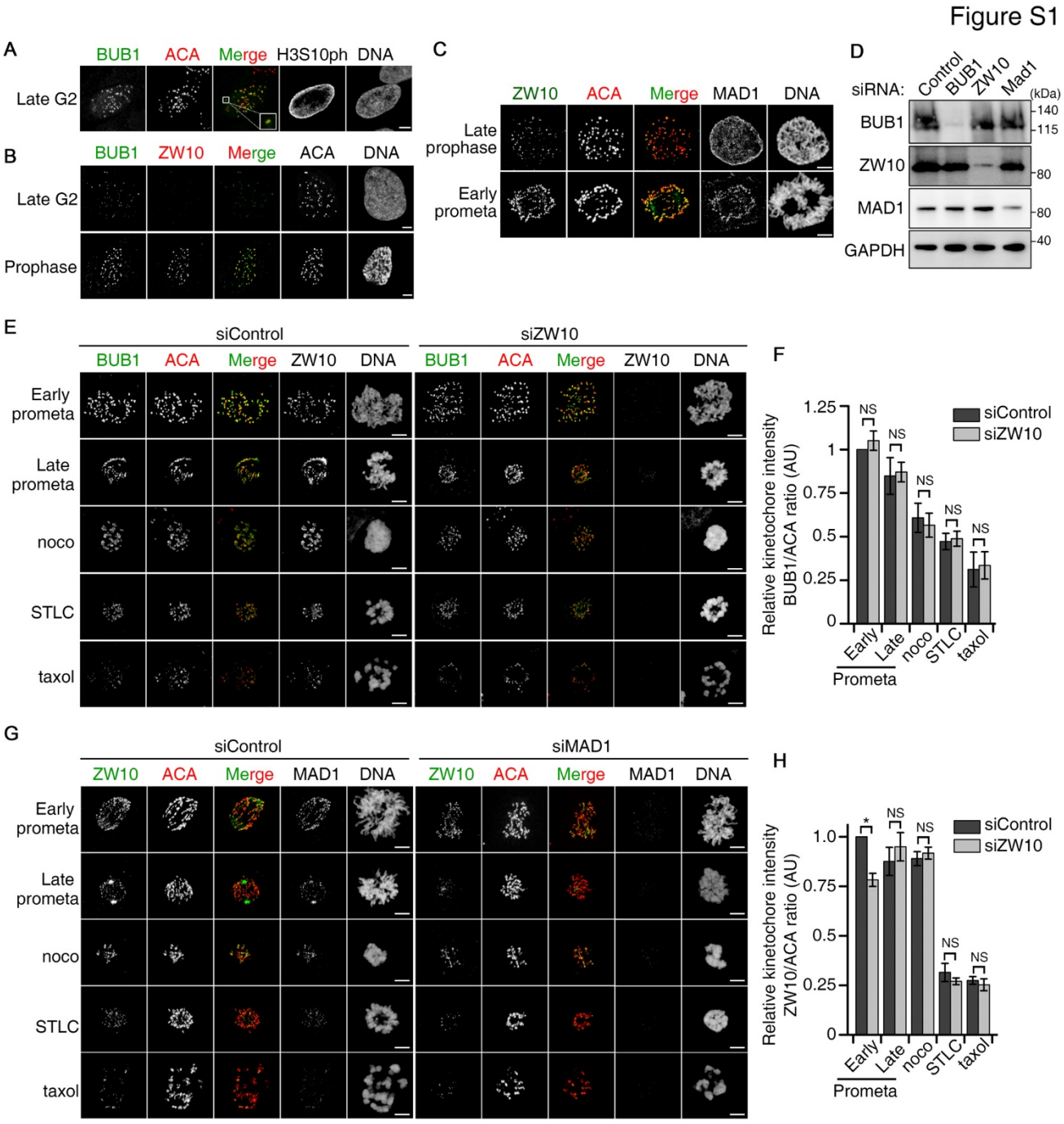

Figure S1. Ordered recruitment of BUB1, RZZ and MAD1 to kinetochores in early mitosis, related to Figure 1.

(A) The kinetochore localization of BUB1 in late G2 coincides with the hyperphosphorylation of histone H3 at Ser10 (H3S10ph) around the nuclear rim. (B) ZW10 is recruited to the kinetochores in prophase, after the recruitment of BUB1. (C) MAD1 is recruited to the kinetochores in early prometaphase, after the recruitment of ZW10. (D) RNAi-mediated knockdown of BUB1, ZW10 or MAD1 in HeLa cells, as detected by immunoblotting. The control refers to the transfection with siRNA for luciferase. (E) HeLa cells treated with the

indicated siRNAs were synchronized to late G2 by sequential thymidine-RO3306 treatments. Subsequently, the cells were released into fresh medium for 10-20 min to obtain cells in early mitosis, or treated with MG132 combined with the indicated drugs for 3h to obtain cells in prolonged prometaphase. (F) Quantification of kinetochore BUB1/ACA ratio in (E). (G) Same as in (E), except for the treatment with different siRNAs. (H) Quantification of the kinetochore ZW10/ACA ratio in (G). In panels A, B, C, E and G the scale bars are 5 μm. In panels F and H, the quantification data represent mean ± SEM from three independent experiments, including at least 10 cells per condition in each experiment. NS: not significant, $^{**}p < 0.01$ with unpaired Student's *t*-test.

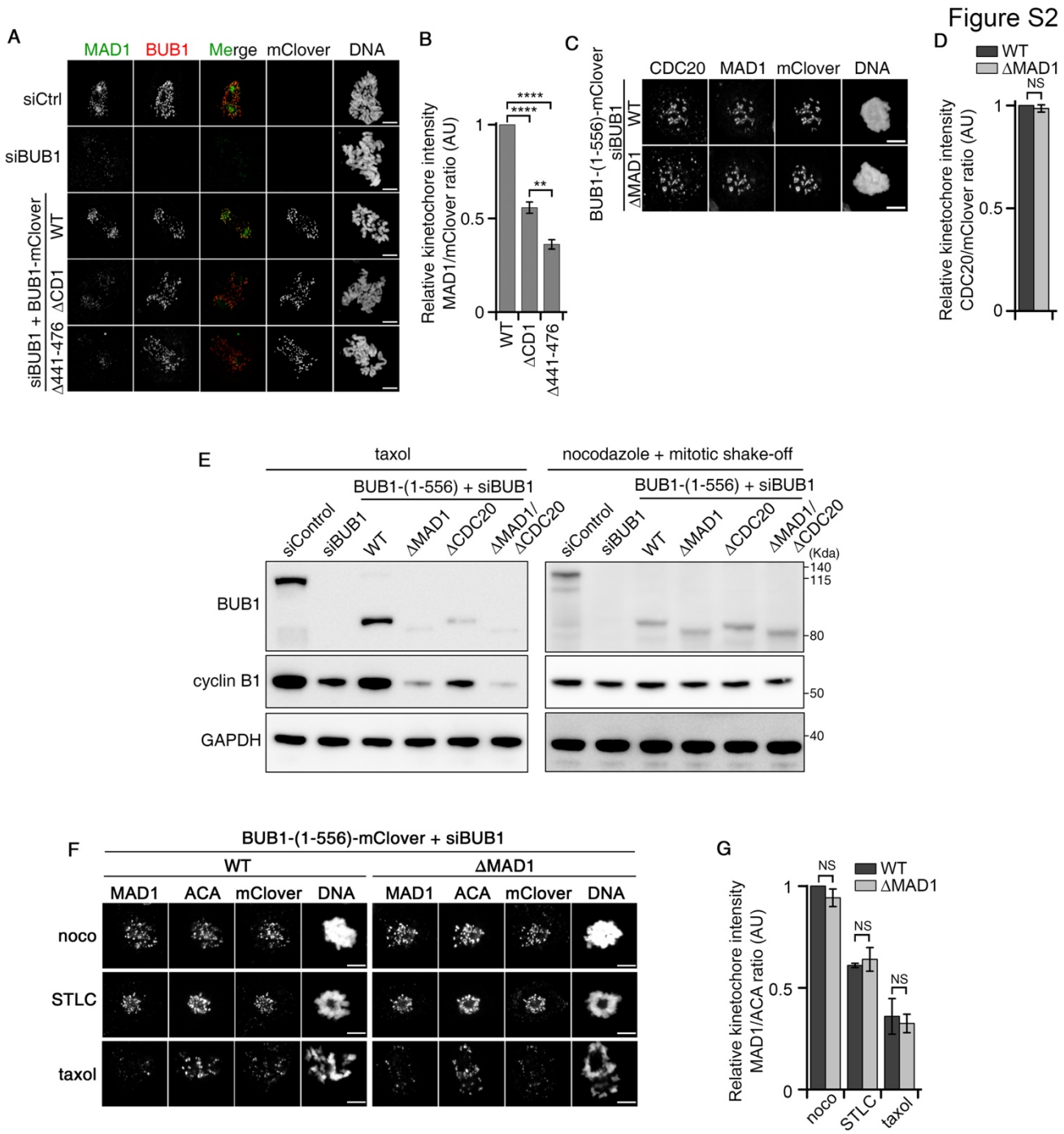

Figure S2. BUB1 is required for MAD1 localization and SAC, related to Figure 2.

(A) One day after the knockdown of endogenous BUB1 (siBUB1), HeLa Flp-in T-REx cell lines expressing mClover-tagged BUB1-(1-556) or the indicated mutants were synchronized to late G2 by sequential thymidine-RO3306 treatments. Subsequently, the cells were released into fresh medium for 10-20 min and MAD1 localization was examined by immunostaining in early prometaphase cells. (B) Quantification of the MAD1/mClover-BUB1 ratios in (A). (C) Hela Flp-in T-REx cell lines expressing mClover-tagged BUB1-(1-556) wildtype (WT) or ΔMAD1 mutant, with knockdown of endogenous BUB1 (siBUB1), were

arrested in mitosis by sequential thymidine-nocodazole treatment, followed by (immuno)staining. (D) Quantification of the kinetochore CDC20/mClover ratio in (C). (E) One day after the knockdown of endogenous BUB1 (siBUB1), HeLa Flp-in T-REx cell lines expressing mClover-tagged BUB1-(1-556) WT or the indicated mutants were treated with thymidine for 24 h and then released into 30 nM taxol for 16 h before immunoblot analysis (left panel). The right panel shows data for similarly treated cells, except for the replacement of taxol with 330 nM nocodazole combined with a mitotic shake-off. (F) Same Hela Flp-in T-REx cell lines as in (C), but arrested in mitosis with nocodazole, STLC or taxol as in Figure 1A. (G) Quantification of the kinetochore MAD1/ACA ratio in (F). In panels (B,D,G), the data are represented as means ± SEM for three independent experiments. For each condition in each experiment at least 10 cells were analyzed. NS: not significant, $p < 0.01$ **, $p < 0.0001$ **** using unpaired Student *t*-test.

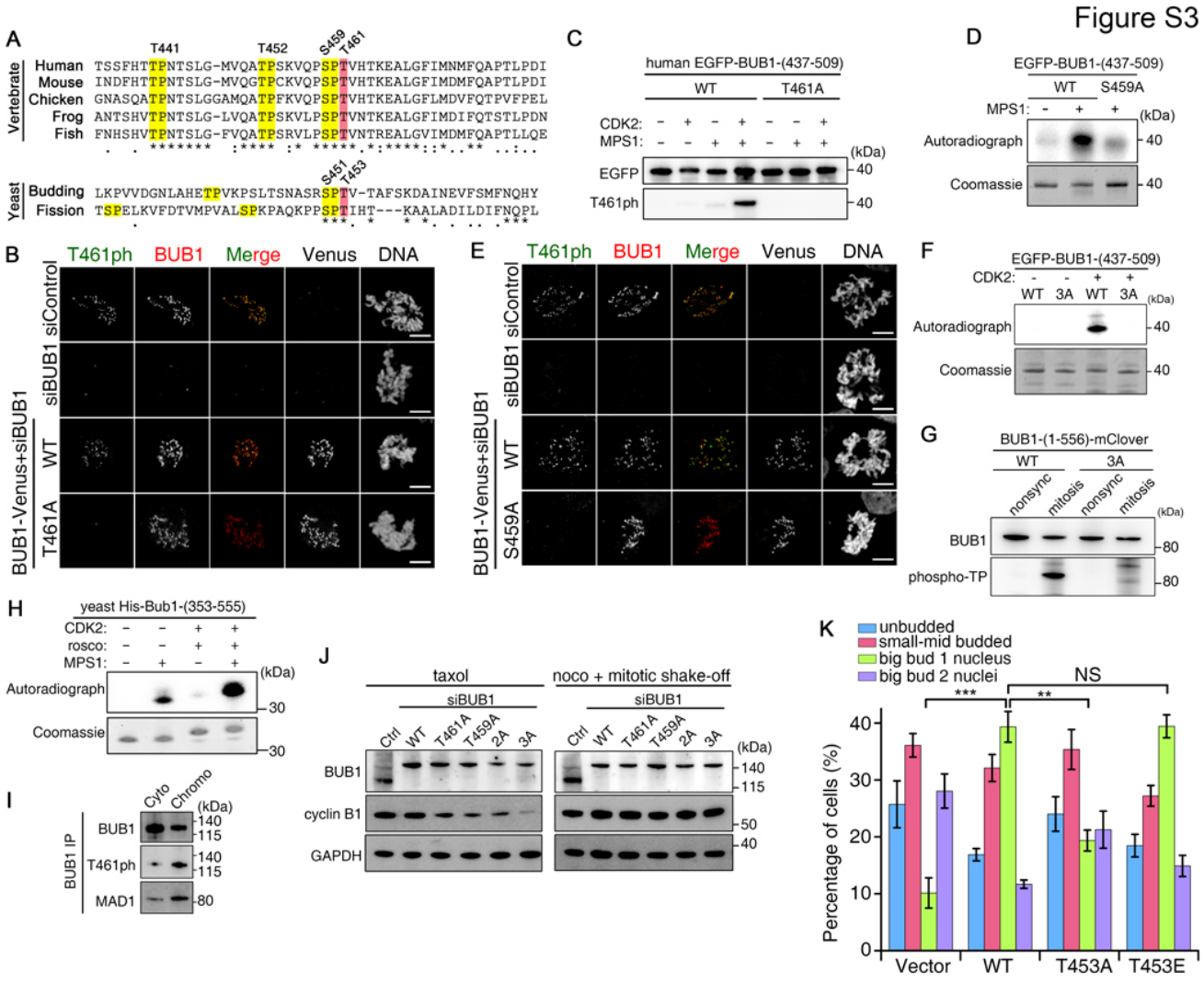

Figure S3. CDK1 and MPS1 phosphorylate the extended CD1 domain of BUB1, related to Figure 3.

(A) Alignment of the sequence of the extended CD1 domain of BUB1 from vertebrates and yeast. (B) HeLa Flp-in T-REx cells expressing Venus-tagged BUB1-WT or BUB1-T461A were treated with control (siControl) or BUB1 siRNA (siBUB1) for 48 h, and synchronized to early prometaphase by sequential thymidine-RO3306 treatment prior to RO3306 release for 20 min. Cells were stained with an antibody raised against a phosphorylated T461 (T461ph) BUB1 peptide. (C) Human EGFP-tagged BUB1-(437-509) WT or BUB1-(437-509)-T461A, purified from HEK293T cells, were incubated for *in vitro* phosphorylation by recombinant MPS1, with or without prior incubation with cyclin-A/CDK2 under phosphorylation conditions. Aliquots were analyzed by immunoblotting. (D) EGFP-traps from HEK293T cells expressing EGFP-tagged BUB1-(437–509)-WT or S459A mutant were first phosphorylated by CDK2 in the presence of cold ATP. After three washes, the traps were further phosphorylated for 1 h by MPS1 in the presence of γ^{32}P-labelled ATP and 25 μM roscovitine, followed by

Coomassie staining and autoradiography. (E) HeLa Flp-in T-REx cells expressing Venus-tagged BUB1-WT or BUB1-S459A were treated with control (siControl) or BUB1 (siBUB1) siRNA for 48 hours, and synchronized to early prometaphase by sequential thymidine-RO3306 treatment prior to RO3306 release for 20 min, followed by (immuno)staining. (F) EGFP-traps from HEK293T cells expressing EGFP-tagged BUB1-(437–509)-WT or the corresponding 3A mutant were phosphorylated with CDK2 in presence of γ^{32}P-labelled ATP and analyzed by Coomassie staining and autoradiography. (G) HeLa cells transiently expressing mClover-tagged BUB1-(1-556)-WT or the corresponding 3A mutant were used either non-synchronized (nonsync) or after synchronization in mitosis by 330 nM nocodazole treatment and mitotic shake-off. Traps of the BUB1 fusions were washed with 2 M NaCl to remove interacting proteins and analyzed by immunoblotting with a phospho-TP antibody. (H) Recombinant His-Bub1-(353-555) from budding yeast was incubated for 1h under conditions of phosphorylation (cold ATP) in the absence or presence of cyclin-A/CDK2. Subsequently, the BUB1 fragment was further phosphorylated for 1 h (γ^{32}P labeled ATP) in the absence or presence of MPS1 and 25 μM of the CDK inhibitor roscovitine (rosco). The samples were analyzed by SDS-PAGE and autoradiography. (I) Late-G2 arrested HeLa cells were released into fresh medium for 15 min before lysis and fractionation into cytosolic (cyto) and chromosomal (chromo) fractions. The chromosomal fraction was solubilized by micrococcal nuclease treatment and sonication. Both fractions were subjected to BUB1 immunoprecipitation before immunoblotting. (J) One day after the knockdown of endogenous BUB1 (siBUB1), HeLa Flp-in T-REx cell lines expressing Venus-tagged BUB1-WT or the indicated mutants were treated with thymidine for 24 h and then released into 30 nM taxol for 16 h before immunoblotting (left panel). Alternatively, the cells were released into 330 nM nocodazole (noco) and collected by shake-off (right panel). (K) Cell-cycle analysis of budding yeast. *SPC105-WT*/bub1Δ cells expressing Bub1-WT or the indicated mutants, under the control of GAL1 promoter, were grown on SC-Gal medium and incubated in the presence of 9.9 μM nocodazole for 4 h. The graph shows the ratio of cells with the indicated morphology. The data are represented as mean percentage ± SEM for three independent experiments. NS: not significant, $^{**}p < 0.01$, $^{***}p < 0.001$, with unpaired Student *t*-test.

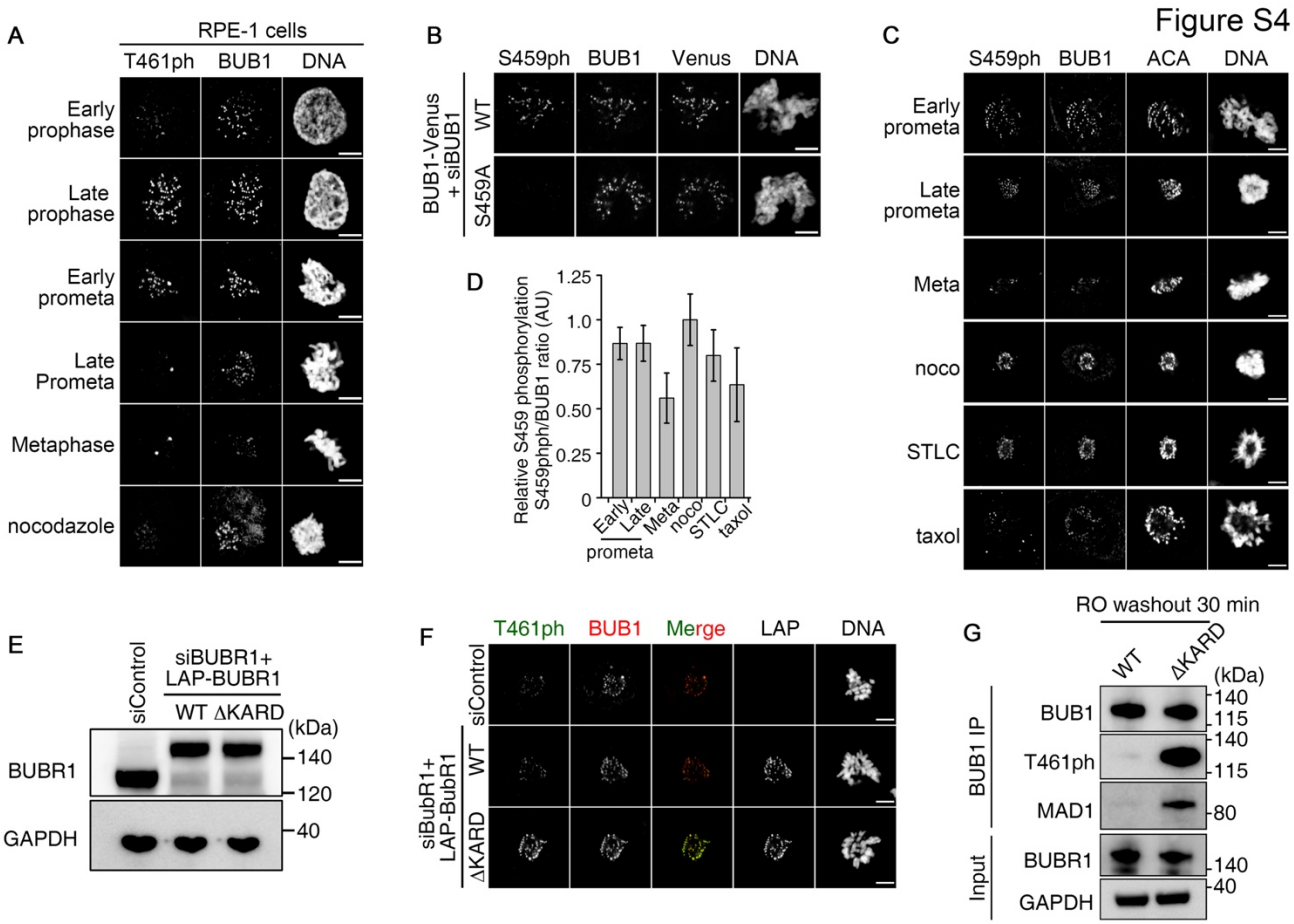

Figure S4. BUBR1-associated PP2A-B56 dephosphorylates BUB1 at T461, related to Figure 4.

(A) RPE-1 cells at different mitotic phases or arrested in nocodazole were stained as indicated. (B) Early prometaphase HeLa Flp-in T-REx cells expressing Venus-tagged BUB1-WT or BUB1-S459A, with knockdown of endogenous BUB1 (siBUB1), were analyzed by (immuno)staining. (C) HeLa cells at different mitotic phases or arrested in nocodazole (noco), STLC, or taxol were stained as indicated. (D) Quantification of BUB1-S459ph/BUB1 ratio in (C). The data represent the mean ± SD for at least 10 cells/condition. (E) Nocodazole-arrested HeLa Flp-in T-REx cells expressing LAP-tagged BUBR1-WT or BUBR1- ΔKARD were treated with a control siRNA (siControl) or BUBR1-siRNA (siBUBR1) for 48 h. The cell lysates were analyzed by immunoblotting. (F) Same as in (E) except that the cells were non-synchronized and late prometaphase cells were stained. (G) Late-G2 arrested HeLa Flp-in T-REx cells expressing LAP-tagged BUBR1-WT or BUBR1-ΔKARD with knockdown of endogenous BUBR1 were released into fresh medium for 30 min before BUB1 immunoprecipitation and immunoblotting.

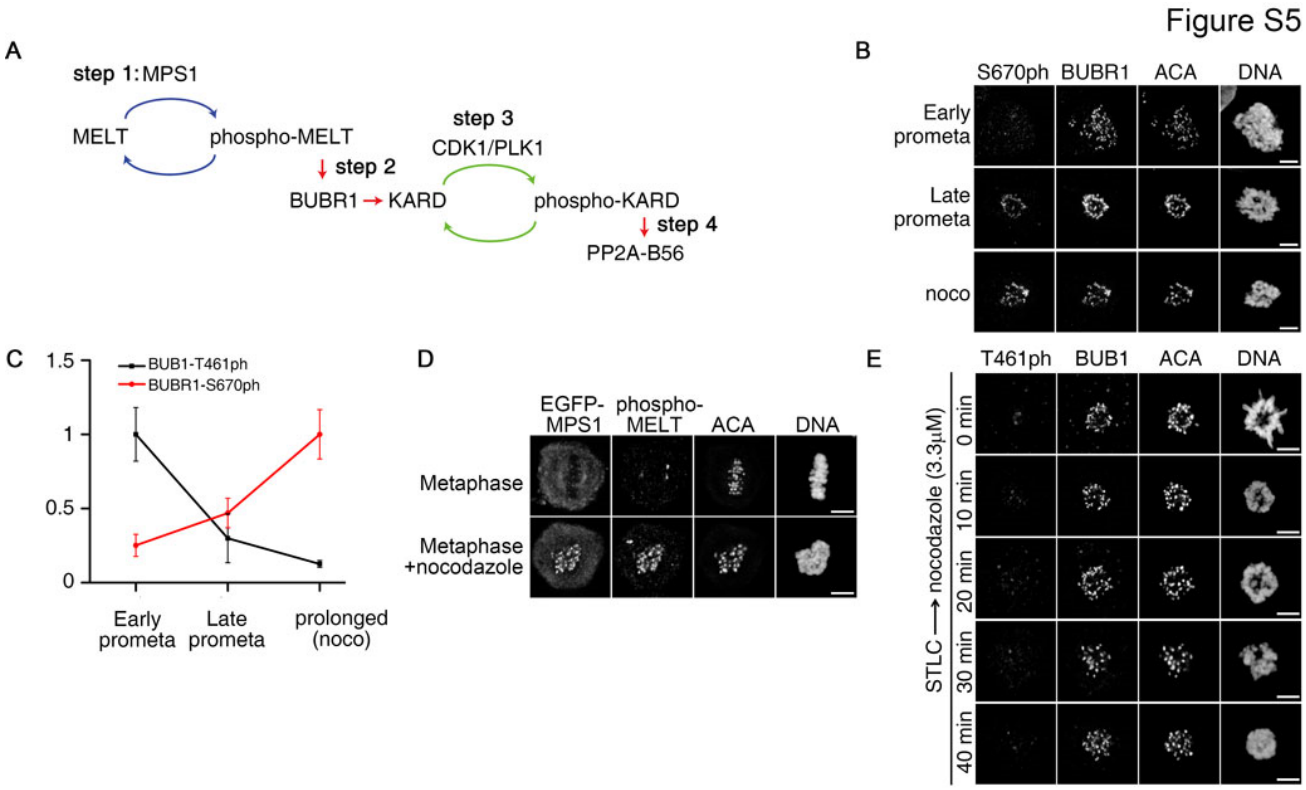

Figure S5. Responsiveness of the BUB1-centered biochemical timer, related to Figure 5. (A) Schematic representation of the time-delay mechanism for the kinetochore recruitment of PP2A-B56 via BUBR1. (B) Immunostaining of BUBR1-S670ph in early prometaphase, late prometaphase or nocodazole-arrested cells. (C) Quantification of BUBR1-S670ph/BUBR1 ratio in (B). The data represent the mean ± SD for at least 10 cells/condition. The BUB1-T461ph/BUB1 ratio was derived from data shown in Figure 4B. (D) HeLa cells transiently expressing EGFP-MPS1 were synchronized in metaphase by releasing monastrol-arrested cells into MG132 for 2 h, followed by an addition of 3.3 μM nocodazole for 10 min. (E) STLC-arrested HeLa cells were treated with 3.3 μM nocodazole for the indicated time before fixation and (immuno)staining.

Figure S6

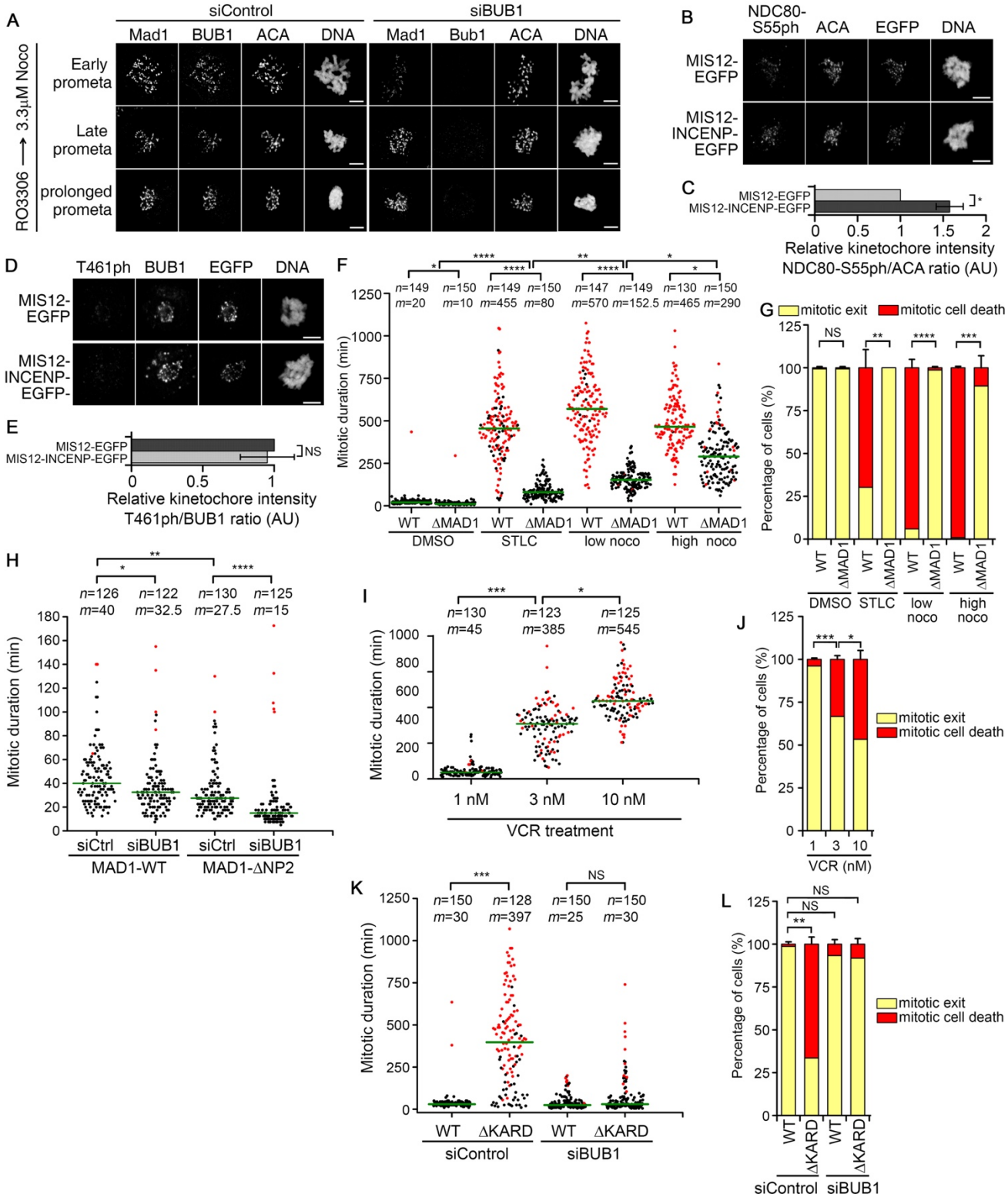

Figure S6. Attachment-independent regulation of MAD1 recruitment via BUB1, related to Figure 6. (A) HeLa cells were first synchronized in G2 with a sequential thymidine-RO3306 treatment. After the RO3306 washout the cells were incubated with 3.3

μM nocodazole before fixation and (immuno)staining. (B and D) HeLa cells transiently expressing MIS12-EGFP or MIS12-INCENP-EGFP were arrested in nocodazole before (immuno)staining. (C and E) Quantification of NDC80-S55ph/ACA and T461ph/BUB1 ratio, respectively. The data are represented as means ± SEM for three independent experiments. For each condition in each experiment at least 10 cells were analyzed. NS: not significant, using unpaired Student *t*-test. (F) Endogenous BUB1 was knocked down in HeLa Flp-in T-REx cells expressing mClover-tagged BUB1-WT or BUB1-ΔMAD1. Cells were synchronized with thymidine for 24 h and released into fresh medium for 6 h prior to treatment with the indicated drugs and DIC time-lapse imaging. *n* indicates number of cells, *m* is the median duration of mitosis (green line) from three independent experiments. (G) Cell fate in (F). The graph shows the mean percentage, error bars indicate SEM from three independent experiments. (H) HCT116 *MAD1L1*-null cells reconstituted with wild-type MAD1-WT or MAD1-ΔNP2, treated with control (siCtrl) or BUB1 siRNA (siBUB1), were synchronized with thymidine for 24 h and released into fresh medium for 6 h prior to DIC time-lapse imaging. (I) HeLa Flp-in T-REx cells expressing LAP-tagged BUBR1-WT combined with knockdown of endogenous BUBR1 were treated with different concentration of vincristine (VCR), as indicated, and subjected to DIC time-lapse imaging. (J) Cell fate in (I). The graph shows the average ± SEM from three independent experiments. (K) Endogenous BUBR1 was knocked down in HeLa Flp-in T-REx cells expressing LAP-tagged BUBR1-WT or BUBR1-ΔKARD, in combination with control (siControl) or BUB1 (siBUB1) knockdown. Cells were synchronized with thymidine for 24 h and released into fresh medium for 6 h prior to DIC time-lapse imaging. (L) Cell fate in (K). The graph shows the mean percentage, error bars indicate SEM from three independent experiments. In panels (F, H, I, K), black dots indicate the duration of mitosis in individual cells, and red dots represent the duration of mitosis in cells that underwent mitotic cell-death. *n* indicates number of cells, *m* is the median duration of mitosis (green line) from three independent experiments. In panels (C, E, F, G, H, I, J, K, L), NS: not significant, **p* < 0.05, ***p* < 0.01, ****p* < 0.001, *****p* < 0.0001 using the unpaired Student's *t*-test.

Figure S7

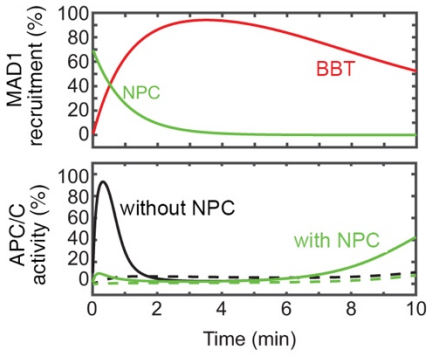

Figure S7. Relative contribution of the NPC and BBT timers at mitotic entry, related to Figure 7. The top panel shows the temporal response of the BBT timer (red), similarly as in Figure 6B, and of the NPC timer (green). In the bottom panel, we then show a simulation of the APC/C activity resulting from either only the BBT timer (black) or the combination of the BBT and NPC timer (green). This is shown for two conditions: the APC/C responds quickly (solid line) or more slowly (dashed line) to the presence of MAD1. One can see that if the APC/C responds too fast, the NPC timer is critical in preventing APC/C activation.

Table S1. List of siRNA oligos, related to Figure 1-6

target	siRNA sequence	supplier	reference
BUB1	GAGUGAUCACGAUUUCUAA	IDT	(Klebig et al., 2009)
ZW10	UGAUCAAUGUGCUGUUCAA	IDT	(Lu et al., 2012)
MAD1	CAGGCAGUGUCAGCAGAAC	IDT	(Zhou et al., 2016)
PP1α	CCGCAUCUAUGGUUUCUAC	Dharmacon	(Qian et al., 2011)
PP1β	UUAUGAGACCUACUGAUGU	Dharmacon	(Qian et al., 2011)
PP1γ	GCAUGAUUUGGAUCUUAUA	Dharmacon	(Qian et al., 2011)
PP2A-Cα	CGUGCAAGAGGUUCGAUGU	Dharmacon	(Qian et al., 2013)
PP2A-B56α	UGAAUGAACUGGUUGAGUA	IDT	(Foley et al., 2011; Nijenhuis et al., 2014)
PP2A-B56β	GAACAAUGAGUAUAUCCUA	IDT	(Foley et al., 2011; Nijenhuis et al., 2014)
PP2A-B56γ	GGAAGAUGAACCAACGUUA	IDT	(Foley et al., 2011; Nijenhuis et al., 2014)
PP2A-B56δ	UCCAUGGACUGAUCUAUAA	IDT	(Foley et al., 2011; Nijenhuis et al., 2014)
PP2A-B56ε	GCACAGCUGGCAUAUUGUA	IDT	(Foley et al., 2011; Nijenhuis et al., 2014)
PP2A-B55α	GCAGAUGAUUUGCGGAUUA	Dharmacon	(Hégarat et al., 2014)
PP2A-B55δ	CAUCCAUAUCCGAUGUAAA	Dharmacon	(Hégarat et al., 2014)
BUBR1-3'UTR	GUCUCACAGAUUGCUGCCU	IDT	(Elowe et al., 2007)
siControl (luciferase)	UAAGGCUAUGAAGAGAUAC	IDT/ Dharmacon	(Qian et al., 2013)

Note: The oligos from IDT were converted into dicer-siRNA format according to the manufacturer's protocol. Isoform-specific siRNA oligos of either PP1, PP2A-B56 or PP2A-B55 were pooled, with an equal amount of siRNA for each isoform.

Table S2. S. cerevisiae strains, related to Figure 3

Strain	Genotype	Reference
CTY10-5d	*MAT*a *ade2 trp1-901 leu2-3*,112 *his3-200 gal4*$^{-}$ *gal80*$^{-}$*URA3*::*lexAop-lacZ*	Dr R. Sternglantz, State University of New York, Stony Brook, NY, USA
M5	*MATa*/*MATα leu2-3,112/leu2-3,112 ura3-52/ura3-52 trp1-92/trp1-92 + /his4*	(Schaaff et al., 1989)
spc105Δ	*spc105Δ::KANMX4*[pRS316-p*GAL1-SPC105-URA3*] in M5α	This work
spc105Δ/bub1Δ	*bub1Δ::TRP1* in *spc105Δ*	This work
SPC105-WT/bub1Δ	*spc105Δ::KANMX4*[pRS315-HA-*SPC105-LEU2*] *bub1Δ::TRP1* derived from *spc105Δbub1Δ* by plasmid shuffling	This work
SPC105-RASA/bub1Δ	*M5spc105Δ::KANMX4*[pRS315-HA-*SPC105RASA-LEU2*] *bub1Δ::TRP1* derived from *spc105Δbub1Δ* by plasmid shuffling	This work

Table S3. Plasmids used in S. cerevisiae, related to Figure 3

Name	Description
pRS316-pGAL1-*SPC105*	*GAL1* promoter driving expression of the *SPC105* complete ORF, tagged at the N-terminus by three HA epitopes, in a pRS316 vector.
pRS316-pGAL1-*SPC105-RASA*	Idem but with *SPC105* mutated at the PP1 binding site (R_{75}VSF). Val and Phe residues, at positions 76 and 79 respectively, have been substituted with Ala.
pRS315-HA-*SPC105*	The *SPC105* physiological promoter followed by the *SPC105* complete ORF, tagged at the N-terminus by three HA epitopes, in a pRS315 vector.
pRS315-HA-*SPC105-RASA*	Idem but with *SPC105* mutated at the PP1 binding site (R_{75}VSF). Val and Phe residues, at positions 76 and 79 respectively, have been substituted with Ala.
pRS316-*pBUB1*	It contains Bub1 promoter, 700 pb upstream from Bub1 ATG driving the expression of BUB1 complete ORF tagged at the N-terminus by three HA epitopes in pRS316 vector.
pRS316-*pBUB1* mutants	Idem but expressing the different Bub1 mutants obtained by directed mutagenesis (T453A or T453E).
pGADT7-*BUB1*	*BUB1* complete ORF subcloned into the *BamHI-XhoI* sites of the pGADT7 (Clontech) yeast two hybrid plasmid.
pGADT7-*BUB1* mutants	Idem but expressing the different Bub1 mutants obtained by directed mutagenesis (S451A, S451E, T453A, T453E).
pBTM-*MAD1*	*MAD1* complete ORF subcloned into the *EcoRI-SalI* sites of pBTM116.

Note: Spc105 and Bub1 mutants were obtained by site directed mutagenesis using Quick-Change Mutagenesis kit and the corresponding mutagenic oligonucleotides according to the manufacturer's protocol. All constructs and mutants were verified by DNA sequencing.